

*Chapter 1*

## EVIDENCE FOR ROOM-TEMPERATURE SUPERCONDUCTIVITY IN CARBON NANOTUBES

*Guo-meng Zhao\**

Department of Physics and Astronomy,  
California State University at Los Angeles, Los Angeles, CA 90032, USA

### Abstract

In this article, we provide electrical, magnetic, tunneling, and Raman spectroscopic evidence for room-temperature superconductivity in carbon nanotubes. Electrical measurements indicate that the superconducting transition temperatures in carbon nanotubes can vary from 0.44 K to 750 K. The temperature dependencies of the resistive transitions agree quantitatively with the well-established Langer-Ambegaokar-McCumber-Halperin (LAMH) theory for the resistive transition of quasi-one-dimensional superconductors. Because of a finite number of transverse conduction channels, the four-probe resistance of an individual tube will not go to zero in the superconducting state. This would lead to a false impression that these tubes are not superconducting. Nonetheless, the on-tube resistance at room temperature is found to be indistinguishable from zero for many individual multi-walled nanotubes. The very small but finite room-temperature on-tube resistance is consistent with quantum phase slips due to the finite number of transverse channels. Magnetic measurements show a small Meissner effect in aligned and physically separated multi-walled nanotubes up to room temperature. The small Meissner effect is due to the fact that the diameter of the tubes is much smaller than the magnetic penetration depth. At low temperatures, the directionally averaged diamagnetic susceptibility for physically coupled multi-walled nanotubes increases by a factor of 4.3 compared with that for physically separated tubes, which is consistent with the enhancement of the Meissner effect due to the Josephson coupling among the superconducting tubes. Further, Raman data and single-particle tunneling spectra consistently show the existence of single particle excitation gaps of larger than 100 meV. We suggest microscopic pairing mechanism for high-temperature superconductivity in carbon nanotubes.

**Keywords:** Room-Temperature Superconductivity, Carbon Nanotubes

---

\*E-mail address: gzhao2@calstatela.edu

## 1. Introduction

It is generally believed that the superconducting transition temperature  $T_c$  cannot be higher than 30 K within the conventional phonon-mediated mechanism. Alexandrov and Mott [1] demonstrate that strong electron-phonon coupling can lead to the formation of intersite bipolarons and that the Bose-Einstein condensation of the bipolarons can explain high-temperature superconductivity in cuprates. Ginzburg [2] and Little [3] propose that high-temperature or room-temperature superconductivity could be realized by exchanging high-energy electronic excitations such as excitons and plasmons. Lee and Mendoza show that superconductivity as high as 500 K can be reached through a pairing interaction mediated by undamped acoustic plasmon modes in a quasi-one-dimensional (1D) electronic system [4]. Moreover, high-temperature superconductivity can occur in a multi-layer electronic system due to an attraction of charge carriers in the same conducting layer via exchange of virtual plasmons in neighboring layers [5]. If the plasmon-mediated pairing mechanisms are relevant, one should be able to find high-temperature superconductivity in quasi-one-dimensional and/or multi-layer systems such as cuprates, carbon nanotubes (CNTs), and graphites.

Carbon nanotubes constitute a novel class of quasi-one-dimensional materials which would offer the potential for high-temperature superconductivity. The simplest single-walled nanotube (SWNT) consists of a single graphite sheet which is curved into a long cylinder with a diameter of about 1 nm. Band-structure calculations predict that carbon nanotubes have two types of electronic structures depending on the chirality [6, 7], which is indexed by a chiral vector  $(n, m)$ :  $n - m = 3N + \nu$ , where  $N, n, m$  are the integers, and  $\nu = 0, \pm 1$ . The tubes with  $\nu = 0$  are metallic while the tubes with  $\nu = \pm 1$  are semiconductive. For metallic chirality SWNTs, there are two and six transverse conduction channels when the Fermi level is crossing the first and second subbands, respectively. Multi-walled nanotubes (MWNTs) consist of at least two concentric shells which could have different chiralities. The outer diameter of MWNTs prepared by arc discharge is normally centered around 10-15 nm. The MWNTs possess both quasi-one-dimensional and multi-layer electronic structures. This unique quasi-one-dimensional electronic structure in both SWNTs and MWNTs make them ideal for plasmon-mediated high-temperature superconductivity.

In order to confirm the existence of superconductivity, it is essential to provide two important signatures: the Meissner effect and the sharp resistive transition to the zero resistance state. However, these two essential signatures are less obvious in a quasi-one-dimensional superconducting wire that has a finite number of transverse conduction channels and a very thin transverse dimension. Due to large superconducting fluctuations, the resistive transition in quasi-1D superconductors could be very broad. Because of the finite number of transverse channels, the four-probe resistance never goes to zero even though the on-wire resistance approaches zero. This would lead to a false impression that these thin wires are not superconducting. Because the magnetic penetration depth may be far larger than the transverse dimension, the diamagnetic Meissner effect might be negligible, which makes it difficult to distinguish between the Meissner effect and orbital diamagnetism. Therefore, it is difficult to unambiguously identify quasi-1D superconductivity in ultra-thin wires such as carbon nanotubes.

In spite of these difficulties to show the conventional signatures of superconductivity in

ultra-thin superconducting wires, Zhao *et al.* [8] reported in 2001 magnetic and electrical evidence for possible superconductivity above room temperature in MWNT mat samples. Since then, Zhao [9, 10, 11, 12, 13, 14] has analyzed the published magnetic, electrical, and optical data for both single-walled and multi-walled carbon nanotubes, and provided over twenty arguments for the existence of superconductivity above room temperature. In this article, we will present electrical, magnetic, tunneling, and Raman spectroscopic evidence for room-temperature superconductivity in carbon nanotubes. In section 2. we make quantitative data analyses on the observed resistive transitions in carbon nanotubes. We find that the resistive transitions in carbon nanotubes agree quantitatively with the Langer-Ambegaokar-McCumber-Halperin (LAMH) theory [15] for quasi-1D superconductors although the superconducting transition temperatures vary from 0.4 K to 750 K for different samples. In section 3., we identify the Meissner effect in the field parallel to the tube axis up to room temperature for aligned MWNTs that are physically separated. The magnitude of the Meissner effect is in quantitative agreement with the predicted penetration depth from the measured carrier density. Furthermore, the diamagnetic susceptibility in closely packed MWNT bundles increases by a factor of over 4 at low temperatures compared with that for physically separated tubes. This is the hallmark of the Josephson coupling among the tubes in bundles. In section 4., we provide Raman spectroscopic evidence for superconductivity at about 665 K in a SWNT mat sample. We quantitatively deduce the superconducting gap  $\Delta(0)$  at zero temperature, the mean-field superconducting transition temperature  $T_{c0}$ , and the electron-phonon coupling constant for the Raman-active graphitic mode. We find that  $\Delta(0) = 106$  meV and  $2\Delta(0)/k_B T_{c0} = 3.7$ . In section 5., we present the tunneling evidence for the existence of large single-particle excitation gaps ( $> 100$  meV) in both SWNTs and MWNTs. In section 6., we provide evidence for negligible on-tube resistances at room temperature in many individual MWNTs, and rule out the possibility of ballistic transport at room temperature. In section 7., we discuss microscopic mechanism for high-temperature superconductivity in carbon nanotubes. We show that SWNT bundles and individual MWNTs are ideal systems for high-temperature superconductivity within the plasmon-mediated mechanism. In section 8., we discuss the pairing symmetry. It appears that s-wave gap symmetry is relevant. In the last section, we will give concluding remarks.

## 2. The Resistive Transitions in Carbon Nanotubes

### 2.1. Theoretical Description for the Resistive Transition in Quasi-1D Superconductors

The phenomenon of superconductivity depends on the coherence of the phase of the superconducting order parameter. The phase coherence of the superconducting order parameter leads to the zero-resistance state. For three-dimensional (3D) bulk systems, the transition to the zero-resistance state occurs right below the mean-field superconducting transition temperature  $T_{c0}$  such that the resistive transition is very sharp and the transition width is negligibly small. In contrast, the resistive transition in quasi-1D superconductors is broad because of large superconducting fluctuations. A quantum theory to describe the resistive transition in quasi-1D superconductors was developed by Langer, Ambegaokar, McCumber

and Halperin [15] over 30 years ago. The theory is based on thermally activated phase slips (TAPS), which cause the resistance to decrease to zero exponentially. In addition to the thermally activated phase slips, there also exist quantum phase slips due to a finite number of transverse channels [16], which prevent ultra-thin wires or tubes from being true superconductors with absolutely zero resistance.

In a theory developed by Langer, Ambegaokar, McCumber and Halperin [15], phase slips occur via thermal activation, leading to a finite width for the resistive transition. The resistance due to the TAPS is given by [17]

$$R_{TA} = \frac{h}{4e^2} \frac{\hbar\Omega}{k_B T} \exp[-\Delta F_o(T)/k_B T], \quad (1)$$

where the attempt frequency  $\Omega$  is [15]

$$\Omega = \frac{\sqrt{3}}{2\pi^{3/2}} \frac{L}{\xi} \sqrt{\frac{\Delta F_o(T)}{k_B T}} \frac{1}{\tau_{GL}}. \quad (2)$$

Here  $L$  is the length of the wire,  $\xi(T)$  is the coherence length, and  $\hbar/\tau_{GL} = (8/\pi)k_B(T_{c0} - T)$ . The barrier energy  $\Delta F_o(T)$  is

$$\Delta F_o(T) = \frac{8\sqrt{2}}{3} \frac{H_c^2(T)}{8\pi} A\xi, \quad (3)$$

where  $H_c^2(T)/8\pi$  is the condensation energy,  $A$  is the cross-section area of the wire, and the critical field near  $T_{c0}$  is given by  $H_c(T) = 1.73H_c(0)(1 - T/T_{c0})$  within the BCS theory [17]. Using  $\xi(T) = \xi(0)(1 - T/T_{c0})^{-1/2}$  (Ref. [17]), we then have

$$\frac{\Delta F_o(T)}{k_B T} = \frac{3cT_{c0}}{T} \left(1 - \frac{T}{T_{c0}}\right)^{3/2}, \quad (4)$$

where

$$c = \frac{\Delta F_o(0)}{k_B T_{c0}} = \frac{8\sqrt{2}}{3} \frac{H_c^2(0)}{8\pi k_B T_{c0}} A\xi(0). \quad (5)$$

Combining the above equations, we finally get

$$R_{TA} = \frac{m}{T^{1.5}} \left(1 - \frac{T}{T_{c0}}\right)^{9/4} \exp\left[-\frac{3cT_{c0}}{T} \left(1 - \frac{T}{T_{c0}}\right)^{3/2}\right], \quad (6)$$

with

$$m = 2.55T_{c0}(3cT_{c0})^{1/2} \frac{L}{\xi(0)}, \quad (7)$$

where  $m$  is in the unit of  $k\Omega K^{3/2}$ . We would like to mention that the exponent in Eq. 6 is factor of 3 larger than that in a similar formula deduced in Ref. [18]. It is possible that the authors in Ref. [18] missed the prefactor of 1.73 in  $H_c(T)$ .

The condensation energy at zero temperature  $H_c^2(0)/8\pi$  is equal to  $N(0)\Delta^2(0)/2$  within the BCS theory, where  $N(0)$  is the density of states near the Fermi level and  $\Delta(0)$  is the superconducting gap at zero temperature. For a single metallic SWNT with two transverse channels,  $N(0)A = 4/3\pi a_{C-C}\gamma_o$  (Ref. [19]),  $\hbar v_F = 1.5a_{C-C}\gamma_o$  (Ref. [20]), where

$\gamma_0$  is the hopping integral and  $a_{C-C}$  (0.142 nm) is the bonding length. Using the BCS relations:  $\xi_{BCS} = \hbar v_F / \pi \Delta(0)$  and  $\Delta(0) / k_B T_{c0} = 1.76$ , and the above relations, one can readily show that

$$c = 0.68 \frac{\xi(0)}{\xi_{BCS}}. \quad (8)$$

If a bundle of single-walled nanotubes or a multi-walled nanotube consists of  $N_{ch}$  transverse channels, then

$$c = 0.34 N_{ch} \frac{\xi(0)}{\xi_{BCS}}. \quad (9)$$

In the clean limit,  $\xi(0) = 0.74 \xi_{BCS}$  and thus  $c = 0.25 N_{ch}$ .

For two-probe or four-probe measurements on carbon nanotubes with finite transverse channels, the total resistance is  $R = R_0 + R_{tube}$ , where  $R_{tube}$  is the on-tube resistance and  $R_0 = R_t = R_Q / t N_{ch}$  for four-probe measurements, or  $R_0 = R_Q / t N_{ch} + R_c$  for two probe measurements [21]. Here  $t$  is the transmission coefficient ( $t \leq 1$ ),  $R_Q = h / 2e^2 = 12.9 \text{ k}\Omega$  is the resistance quantum,  $R_c$  is the contact resistance, and  $R_t$  is the tunneling resistance. Both  $R_c$  and  $R_t$  should be temperature independent. For ideal contacts,  $R_c = 0$  and  $t = 1$ , so  $R_0 = R_t = 12.9 \text{ k}\Omega / N_{ch}$  for a bundle comprising  $N_{ch}$  transverse channels. For quasi-1D systems,  $N_{ch}$  is always finite such that both four-probe and two-probe resistances never go to zero even if the on-tube resistance is zero. Only if  $N_{ch}$  goes to infinity, as in the bulk 3D systems,  $R_t$  becomes zero such that four probe resistance can go to zero below the superconducting transition temperature. Therefore, the non-zero four-probe resistance in ultra-thin wires does not rule out superconductivity in the wires.

## 2.2. The Resistive Transition in a SWNT Bundle with $T_{c0} = 0.44 \text{ K}$

In 2001, Kociak *et al.* provided the first experimental evidence for superconductivity in single-walled carbon nanotube bundles from the electrical transport measurements [22]. Although the superconducting transition temperature is low ( $< 1 \text{ K}$ ), the resistive behavior of the nanotube bundle can serve as a prototype for the resistive transition in quasi-1D superconducting wires with a finite number of transverse conduction channels.

Figure 1 shows the two-probe resistance data for a SWNT bundle that consists of about 350 tubes [22]. One can see that the resistance starts to drop below about 0.5 K, decreases more rapidly below  $T_{c0} \simeq 0.44 \text{ K}$  and saturates to a value of 74  $\Omega$ . From the saturated value of  $R_0 = 74 \Omega$  and the relation:  $R_0 = R_Q / t N_{ch} + R_c$ , one can easily find that more than 174 transverse channels are connected to the electrodes and participate in electrical transport. This implies that more than 87 metallic-chirality superconducting SWNTs take part in electrical transport. Considering the fact that one third of tubes should have metallic chiralities and become superconducting, we find the total number ( $N_m$ ) of the superconducting tubes to be 117, implying that  $t \geq 0.74$ .

The value of  $N_m$  can be also deduced from the measured current  $I_c^*$  at which the last resistance jump occurs. The  $I_c^*$  corresponds to the critical current for a superconducting wire without disorder and with the same number of transverse channels [22]. According to the BCS theory, the mean-field critical current in the clean limit is given by [17]  $I_c^*(0) = en_s A \Delta(0) / \hbar k_F$ . The superfluid density  $n_s$  is equal to the normal-state carrier density  $n$  which is given by  $n = 2N_m N(0) E_F = 2N_m N(0) \hbar v_F k_F = 4N_m k_F / A\pi$ . Here we have

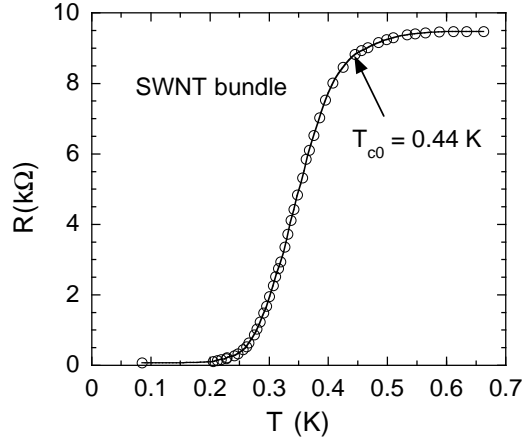


Figure 1. The temperature dependence of the two-probe resistance for a SWNT bundle that consists of about 350 tubes. The data are extracted from Ref. [22].

used the relations for single metallic tube:  $N(0)A = 4/3\pi a_{C-C}\gamma_0$ ,  $\hbar v_F = 1.5a_{C-C}\gamma_0$ , and  $E = \hbar v_F|k|$ . Using  $\Delta(0)/k_B T_{c0} = 1.76$ , we finally get  $I_c^* = 7.04k_B T_{c0} N_m / e R_Q$ . With  $I_c^* = 2.4 \mu\text{A}$  (Ref. [22]) and  $T_{c0} = 0.44 \text{ K}$ , we have  $N_m = 116$ , in remarkably good agreement with the value (117) deduced above.

In Fig. 2, we fit the resistance data below  $0.88T_{c0}$  by

$$R = R_o + \alpha \exp\left[-\frac{3\beta T_c^*}{T} \left(1 - \frac{T}{T_c^*}\right)^{3/2}\right]. \quad (10)$$

Here the first term  $R_o = 74 \Omega$  is the sum of the tunneling and contact resistances and the second term is the on-tube resistance, which has a similar exponential dependence on  $T$  as Eq. 6 but with a temperature independent prefactor. We can see that the fit is excellent with the fitting parameter  $\beta = 2.99 \pm 0.05$  and  $T_c^* = 0.394 \pm 0.002 \text{ K}$ . Reducing or increasing the temperature region for the fit tends to worsen the fit quality. Therefore, the on-tube resistance goes to zero exponentially below  $T_c^* = 0.89T_{c0}$ . The microscopic origin of this simple exponential dependence up to  $0.89T_{c0}$  is not clear, so we consider Eq. 10 only as an empirical formula.

We also try to fit the resistance below  $0.88T_{c0}$  by

$$R = R_o + \frac{m}{T^{1.5}} \left(1 - \frac{T}{T_{c0}}\right)^{9/4} \exp\left[-\frac{3cT_{c0}}{T} \left(1 - \frac{T}{T_{c0}}\right)^{3/2}\right]. \quad (11)$$

Here the first term  $R_o = 74 \Omega$  and the second term is the on-tube resistance which is the same as Eq. 6 predicted by the LAMH theory. We find that the fit is not good and the fitting parameters have no quantitative agreement with the LAMH theory. This is because the LAMH theory is only applied to the temperature region where the barrier height is far larger than  $k_B T$  so that current carrying states involved are truly metastable [23]. The estimated region of validity for the LAMH theory is below  $0.07R_N$  for dirty wires where the mean free path  $l \ll \xi_{BCS}$  (Ref. [23]). For the SWNT bundle, the condition of  $l \ll \xi_{BCS}$  is well satisfied, as seen below. In Fig. 3, we fit the resistance data below  $0.06R_N$  by

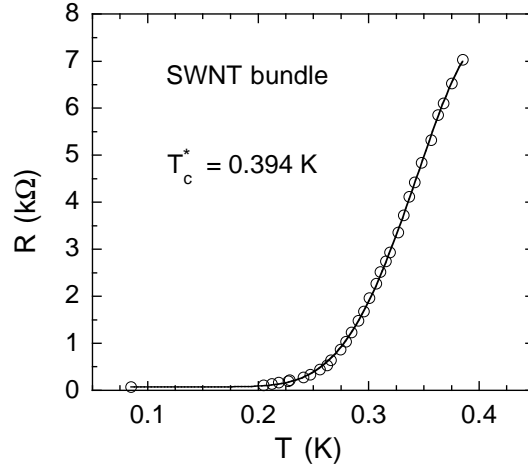


Figure 2. The temperature dependence of the two-probe resistance for a SWNT bundle below  $0.88T_{c0}$ . The solid line is the curve best fitted by Eq. 10 with  $\beta = 2.99 \pm 0.05$  and  $T_c^* = 0.394 \pm 0.002$  K. Reducing or increasing the temperature region for the fit tends to worsen the fit quality. It is striking that the on-tube resistance below  $0.88T_{c0}$  decreases exponentially to zero.

Eq. 11. Here we have ignored the normal conduction because  $R_{TA}$  is a factor of about 20 smaller than  $R_N$ . One can see that the fitting is very good with the fitting parameters:  $m = 26.6 \pm 4.7 \text{ k}\Omega\text{K}^{1.5}$  and  $c = 3.08 \pm 0.13$ . It is remarkable that the value of  $c$  is nearly the same as the value of  $\beta$  ( $2.99 \pm 0.05$ ) deduced above from a simple exponential fit (Eq. 10). We will see below that the fitting parameters  $c$  and  $m$  are in quantitative agreement with the LAMH theory.

From the values of  $m$ ,  $c$ , and  $T_{c0}$ , we can evaluate the zero-temperature coherence length  $\xi(0)$  using Eq. 7. Substituting  $m = 26.6 \text{ k}\Omega\text{K}^{1.5}$ ,  $c = 3.08$ ,  $T_{c0} = 0.44$  K, and  $L = 10000 \text{ \AA}$  into Eq. 7, we obtain  $\xi(0) = 850 \text{ \AA}$ . From the measured  $R_N(0.25\text{K})/L = 12 \text{ k}\Omega/\mu\text{m}$  (Ref. [22]) and the relation  $R_N/L = R_Q/2N_m l$  (Ref. [24]), we can calculate the mean free path  $l$  at 0.25 K. With  $N_m = 117$ , we get  $l = 46 \text{ \AA}$ . Substituting  $l = 46 \text{ \AA}$  and  $\xi(0) = 850 \text{ \AA}$  into the dirty-limit formula [23]:  $\xi(0) = 0.85\sqrt{\xi_{BCS}l}$ , we have  $\xi_{BCS} = 21739 \text{ \AA}$ . With  $\xi_{BCS} = 21739 \text{ \AA}$ ,  $\xi(0) = 850 \text{ \AA}$ , and  $N_{ch} = 2N_m = 334$ , we calculate  $c = 3.11$  from Eq. 9. It is remarkable that the calculated value of  $c$  from Eq. 9 is in quantitative agreement with the value (3.08) deduced from the fitting.

We can also estimate the Fermi velocity  $v_F$  from the deduced value of  $\xi_{BCS}$  and the formula  $\xi_{BCS} = 0.18\hbar v_F/k_B T_{c0}$ . With  $\xi_{BCS} = 21739 \text{ \AA}$  and  $T_{c0} = 0.44$  K, we get  $\hbar v_F = 4.6 \text{ eV}\text{\AA}$ . Then we estimate  $\gamma_o = 2.16 \text{ eV}$  from  $\hbar v_F = 1.5a_{C-C}\gamma_o$ . This value is very close to the value (2.4 eV) estimated from the first-principle calculation [25].

The deduced value of  $\xi(0) = 850 \text{ \AA}$  is also in excellent agreement with the measured critical current  $I_c$  for this SWNT bundle. For a diffusive superconducting wire, the critical current  $I_c$  is given by [26]

$$I_c = \frac{\Delta(0)}{eR_N} \frac{L}{\xi(0)}. \quad (12)$$

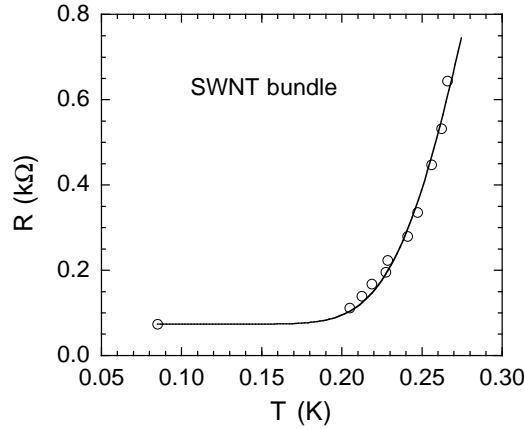


Figure 3. The temperature dependence of the two-probe resistance for a SWNT bundle below  $0.06R_N$ . The solid line is the curve fitted to the data below  $0.06R_N$  by Eq. 11 predicted by the LAMH theory. The estimated region of validity for the LAMH theory is below  $0.07R_N$  for dirty wires where  $l \ll \xi_{BCS}$  (Ref. [23]). The condition of  $l \ll \xi_{BCS}$  is well satisfied in the SWNT bundle (see text).

Using  $\Delta(0) = 1.76k_B T_{c0}$  and substituting  $R_N(0.1\text{K})/L = 12.5 \text{ k}\Omega/\mu\text{m}$  (Ref. [22]) and  $\xi(0) = 850 \text{ \AA}$  into Eq. 12, we find  $I_c = 62.4 \text{ nA}$ , which is very close to the measured value (62 nA) at 0.1 K (Ref. [22]). Thus, the resistance data of the SWNT bundle agrees with the LAMH theory in a quantitative way.

### 2.3. The Resistive Transition in an Individual MWNT with $T_{c0} = 262 \text{ K}$

In 1996, Ebbesen *et al.* made four-probe resistance measurements on individual multi-walled carbon nanotubes [27]. Four 80-nm-wide tungsten leads were patterned by ion-induced deposition of tungsten from  $\text{W}(\text{CO})_6$  carrier gas. This technique makes it possible for electrodes to connect multi-shells of the tubes [28]. It is interesting that the electrical properties vary significantly from samples to samples. Some tubes show abrupt jumps in resistivity when the temperature increases. In some other tubes, the resistance at room temperature is very small (e.g., 200  $\Omega$ ) but a metal-insulator transition occurs below about 200 K. We will show that the resistive behavior in the former case is in quantitative agreement with that expected for quasi-1D superconductivity. The resistive behavior in the latter case may be explained by a superconductor-to-insulator transition in dirty quasi-1D systems.

Figure 4 shows the four-probe resistance data for a single MWNT with a diameter of  $12 \pm 2 \text{ nm}$ . The inner contact distance is  $L = 5000 \text{ \AA}$ . One can see that the resistance drops more rapidly below about 262 K and saturates to a value of about 8.80 k $\Omega$  below 160 K. The resistive behavior of this single tube is similar to the resistive transition for a quasi-1D superconductor with  $T_{c0} \simeq 262 \text{ K}$ . The finite resistance far below the superconducting transition temperature is due to a finite number of transverse channels, which is estimated to be about 54 for this tube (see below). Using  $R_0 = 8.80 \text{ k}\Omega$ ,  $N_{ch} = 54$ , and the relation:  $R_0 = R_Q/tN_{ch}$ , we estimate the average  $t$  for each channel to be about 0.013. The small value of  $t$  suggests that the electrical contacts to the tube are rather poor. Assuming a negligible

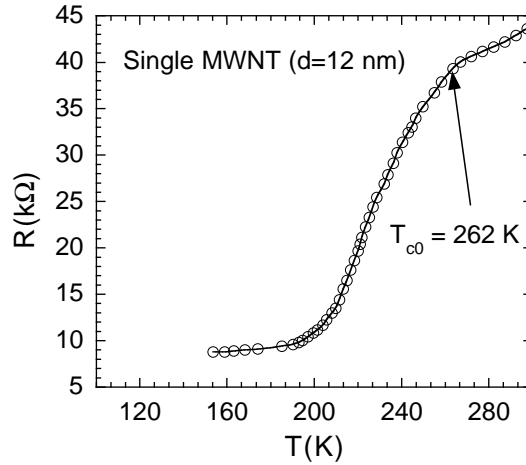


Figure 4. The temperature dependence of the resistance for a single MWNT with  $d \simeq 12$  nm. The data are extracted from Ref. [27].

on-tube resistance below 160 K, we estimate that the on-tube resistance in the normal state (at 300 K) is about 34 kΩ, leading to  $R_N/L = 68$  kΩ/μm.

In Fig. 5 we fit the resistance data below  $T = 233$  K =  $0.89T_{c0}$  by Eq. 10 with a fixed  $R_0 = 8.80$  kΩ. One can see that the fitting is excellent with the fitting parameters:  $\beta = 11.71 \pm 0.12$ ,  $\alpha = 19.0 \pm 0.1$  kΩ, and  $T_c^* = 234$  K. It is interesting that  $T_c^* = 0.89T_{c0}$ , which is the same as that for the SWNT bundle with  $T_{c0} = 0.44$  K.

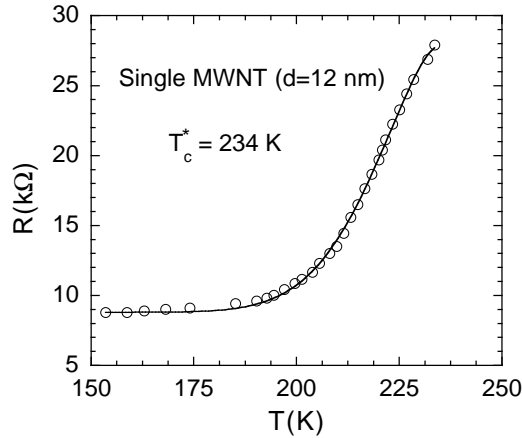


Figure 5. The temperature dependence of the resistance for the 12-nm MWNT below 233 K =  $0.89T_{c0}$ . The solid line is the curve best fitted by Eq. 10 with the fitting parameters:  $\beta = 11.71 \pm 0.12$ ,  $\alpha = 19.0 \pm 0.1$  kΩ, and  $T_c^* = 234$  K, and with a fixed  $R_0 = 8.80$  kΩ. Reducing or increasing the temperature region for the fit tends to worsen the fit quality.

In Fig. 6 we fit the resistance data below about  $0.15R_N$  by

$$R = R_0 + \frac{m}{T^{1.5}} \left(1 - \frac{T}{T_{c0}}\right)^{9/4} \exp\left[-\frac{3cT_{c0}}{T} \left(1 - \frac{T}{T_{c0}}\right)^{3/2}\right]. \quad (13)$$

We fit the resistance data in this region because  $l \simeq \xi_{BCS}$ , as seen below. We can see that the fitting is excellent between 190 K and 210 K. There is a small deviation between 160 and 190 K, which may arise from quantum phase slips. The fitting parameters are  $m = (1.64 \pm 0.14) \times 10^7 \text{ k}\Omega\text{K}^{1.5}$  and  $c = 10.27 \pm 0.23$ . It is striking that the values of  $\beta$  and  $c$  are also very close, similar to the case of the SWNT bundle with  $T_{c0} = 0.44 \text{ K}$ .

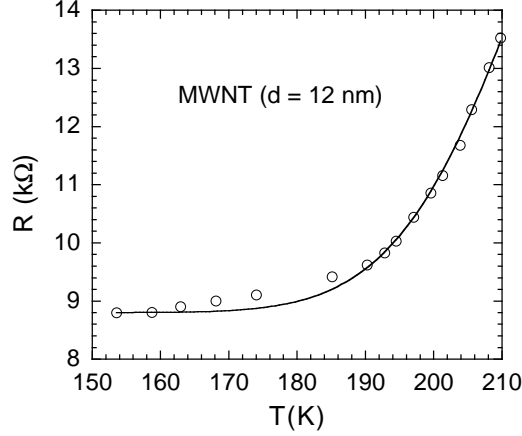


Figure 6. The temperature dependence of the resistance for the 12-nm MWNT below about  $0.15R_N$ . The solid line is the curve best fitted by Eq. 13 with the fitting parameters:  $m = (1.64 \pm 0.14) \times 10^7 \text{ k}\Omega\text{K}^{1.5}$  and  $c = 10.27 \pm 0.23$ .

From the values of  $m$ ,  $c$ , and  $T_{c0}$ , we can evaluate the zero-temperature coherence length  $\xi(0)$  using Eq. 7. Substituting  $m = 1.64 \times 10^7 \text{ k}\Omega\text{K}^{1.5}$ ,  $c = 10.27$ ,  $T_{c0} = 262 \text{ K}$ , and  $L = 5000 \text{ \AA}$  into Eq. 7, we obtain  $\xi(0) = 18.3 \text{ \AA}$ . From the measured  $R_N/L = 68 \text{ k}\Omega/\mu\text{m}$  and the relation  $R_N/L = R_Q/N_{ch}l$  (Ref. [24]), we calculate  $N_{ch}l = 1897 \text{ \AA}$ . Substituting  $c = 10.27$  into Eq. 9, we get  $N_{ch} = 30.2\xi_{BCS}/\xi(0)$ . By solving the three equations:  $N_{ch}l = 1897 \text{ \AA}$ ,  $N_{ch} = 30.2\xi_{BCS}/\xi(0)$ , and  $\xi(0) = 0.74\xi_{BCS}\sqrt{\chi(0.882\xi_{BCS}/l)}$ , we finally obtain  $l = 35 \text{ \AA}$ ,  $N_{ch} = 54$ , and  $\xi_{BCS} = 33.0 \text{ \AA}$ . Here the Gorkov function  $\chi(x)$  is defined as [23]

$$\chi(x) = \sum_{n=0}^{\infty} \frac{0.95}{(1+2n)^2(1+2n+x)}. \quad (14)$$

The fact that  $l \simeq \xi_{BCS}$  indicates that the LAMH theory (Eq. 13) is valid only below  $0.17R_N$  (Ref. [23]). This justifies the region of the data we select to fit.

We can also evaluate the Fermi velocity  $v_F$  from the deduced value of  $\xi_{BCS}$  and the formula  $\xi_{BCS} = 0.18\hbar v_F/k_B T_{c0}$ . With  $\xi_{BCS} = 33 \text{ \AA}$  and  $T_{c0} = 262 \text{ K}$ , we get  $\hbar v_F = 4.14 \text{ eV}\text{\AA}$ , which is about 10% smaller than that deduced above for the SWNT bundle. Using the value of  $\gamma_0 = 2.4 \text{ eV}$  estimated from the first principle calculation [25] and the relation  $\hbar v_F = 1.5a_{C-C}\gamma_0$  (Ref. [20]) for the first subband of metallic chirality tubes, we obtain  $\hbar v_F = 5.1 \text{ eV}\text{\AA}$ . The value of  $\hbar v_F$  deduced from the LAMH theory is about 20% lower than the value expected for the first subband of metallic chirality tubes. Such a small discrepancy may be explained by a fact that the Fermi level of some outer shells is crossing the second or higher subbands where [29] the Fermi velocity is smaller than that for the first

subband. This quantitative agreement provides compelling evidence for high-temperature superconductivity at 262 K in this 12-nm MWNT.

Now we would like to show that the deduced  $N_{ch} = 54$  is also reasonable. For the MWNT with  $d = 12$  nm, the total number of shells can be estimated to be about 17 using the fact that the intershell distance is 0.34 nm. This implies that the average number of conducting channels per shell is about 3.2. This is possible when the Fermi level of some outer shells crosses their second subband (see above), which have 6 channels for a metallic chirality shell and 4 channels for a semiconducting chirality shell [20].

We can estimate the lower limit of the average number of conducting channels per shell for an 18-nm MWNT from the measured room-temperature four-probe resistance, which is  $200 \Omega$  (Ref. [27]). Using the relation  $R = R_Q/tN_{ch} + R_{tube} \geq R_Q/N_{ch}$  and  $R = 200 \Omega$ , we get  $N_{ch} \geq 64$ . The total number of shells for the 18-nm MWNT should be about 26. This implies that the average number of conducting channels per shell for the 18-nm MWNT is larger than 2.5, in agreement with that (3.2) deduced independently for the 12-nm MWNT.

The other puzzling feature in the resistive behavior of this 18-nm MWNT is the metal-insulator transition below about 200 K (Ref. [27]). We can attribute this to a superconductor-insulator transition in dirty quasi-1D systems. It is shown that when the thermal length is larger than the localization length below a temperature  $T_{loc}$  in quasi-1D systems, the Anderson localization sets in and the ground state becomes insulating [30].

#### 2.4. The Resistive Transition in a SWNT Mat with $T_{c0} = 710$ K

Single-walled carbon nanotubes, prepared by metal-catalysed laser ablation of graphite, form closely-packed crystalline bundles. The bulk samples, or mats consist of entangled bundles that are contacted with each other and oriented randomly [31]. If close-packed crystalline bundles are superconductors, the bulk samples should behave like granular superconductors. Depending on the Josephson coupling strength between the superconducting “grains”, the ground state could be metallic, insulating, or superconducting [32]. It is interesting that the contact barrier resistance of a granular superconductor follows a rather unusual exponential temperature dependence in a certain temperature range [32], that is,  $R_b(T) = R_b(0) \exp(BT)$ , where  $B$  could be positive, negative, or zero. This temperature dependence of the barrier resistance was also suggested [33] for the intertube barrier resistance in MWNTs. The barrier resistance extrapolated to zero temperature is finite even if the  $T$ -dependence of the resistance behaves like an insulator. This unique resistive behavior makes a clear distinction from that for conventional semiconductors where the resistance at zero temperature goes to infinity.

Figure 7 shows the temperature dependence of the resistivity for a SWNT mat. The data are extracted from Ref. [31]. Below 200 K the resistivity is nearly temperature independent while above 200 K the resistivity increases suddenly and starts to flatten out above 550 K. This behavior is similar to that for a granular superconductor. Below we will show that this is indeed the case.

We fit the resistivity data by

$$\rho = \rho_0(T) + \alpha \exp\left[-\frac{3\beta T_c^*}{T} \left(1 - \frac{T}{T_c^*}\right)^{3/2}\right]. \quad (15)$$

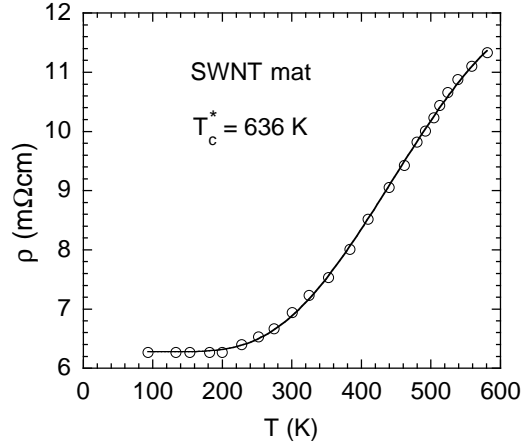


Figure 7. The temperature dependence of the resistivity for a SWNT mat. The data are extracted from Ref. [31]. The solid line is the curve fitted by Eq. 15 with the fitting parameters:  $\rho_0 = 6.277 \pm 0.018$  mΩcm,  $\beta = 0.90 \pm 0.04$ , and  $T_c^* = 636.3$  K.

Here the first term is the intertube contact barrier resistivity, which could be temperature dependent, and the second term is the on-tube resistivity that follows a simple exponential form same as Eq. 10. In the present case, the intertube barrier resistivity appears to be independent of temperature in the temperature region we are interested in, i.e.,  $B \simeq 0$ . It is striking that the data can be well fitted by Eq. 15 with the fitting parameters:  $\rho_0 = 6.277 \pm 0.018$  mΩcm,  $\beta = 0.90 \pm 0.04$ , and  $T_c^* = 636.3$  K. Using the relation  $T_c^* = 0.895T_{c0}$  deduced empirically above, we obtain  $T_{c0} = 710$  K. It is remarkable that the  $T_{c0}$  value obtained from the resistivity data is very close to that (665 K) inferred from the Raman data for a similarly prepared SWNT mat [13, 14] (see section 4.).

By extrapolation of the data shown in Fig. 7 to  $T = 710$  K, we estimate the normal-state on-tube resistivity at 710 K to be  $\rho_N^{exp} \simeq 1.1\rho_N^{exp}(T_{c0}) = 6270$  μΩcm. Since about one-third of tubes have metallic chiralities and the mat consists of crystalline bundles that are oriented randomly, the intrinsic normal-state on-tube resistivity  $\rho_N^i$  of the superconducting tubes should be much smaller than  $\rho_N^{exp}$ , that is,  $\rho_N^i = \rho_N^{exp}/f$ , where  $f$  is the reduction factor that should be close to  $3(1/0.33) = 9$ . The intrinsic mean free path  $l$  is related to  $\rho_N^i$  by

$$l = \frac{R_Q A_o}{2 \rho_i}, \quad (16)$$

were  $A_o$  is the area of single tube, which is equal to  $1.54 \times 10^{-18}$  m<sup>2</sup> for  $d = 1.4$  nm. If we take  $f = 9$ , we get  $l = 14$  Å at  $T = 710$  K from Eq. 16. If the resistivity jump above 200 K were due to inelastic scattering, the inelastic mean free path would be about 14 Å at about 700 K. This is inconsistent with any electrical transport mechanism for SWNTs.

Using  $\hbar v_F = 4.5$  eVÅ and  $T_{c0} = 710$  K, we find that the BCS coherence length along the tube-axis direction  $\xi_{BCS} = 13.2$  Å. The zero-temperature coherence length along the tube-axis direction  $\xi(0)$  should be smaller than the clean-limit value:  $0.74\xi_{BCS} = 10$  Å. Then the coherence length perpendicular to the tube axis should be order of 1 Å. Such a short coherence length implies that only those superconducting tubes that are adjacent

to each other can have enough Josephson coupling to form a superconducting bundle. A simulation [34] indicates that the average number of the metallic-chirality tubes that are adjacent to each other is about 2. This implies that the average number of the metallic-chirality tubes comprising a superconducting bundle is also about 2, and that there are a number of independent superconducting bundles within a physical bundle.

If we assume that the normal-state resistivity is linearly proportional to  $T$  above 200 K, the average mean-free path between 200 K and 580 K should be about 26 Å, significantly larger than  $\xi_{BCS}$ . Then we estimate  $\xi(0) \simeq 8$  Å. Using Eq. 9 and  $c \simeq \beta = 0.9$ , we obtain  $N_{ch} \simeq 4.5$ . This implies that, on average, about two metallic chirality tubes are adjacent to each other and form a superconducting bundle, in quantitative agreement with the simulation [34].

## 2.5. The Resistive Transition in a MWNT Mat with $T_{c0} = 752$ K

A multi-walled carbon nanotube is packed in such a way that each shell is concentric with each other. If each shell has phase-incoherent superconductivity, MWNTs are almost optimally packed to maximize the Josephson coupling and phase coherence. Individual MWNTs can be closely packed into bundles. The bulk samples, or mats are made of entangled bundles that are contacted with each other and oriented randomly. The bulk samples should also behave like granular superconductors.

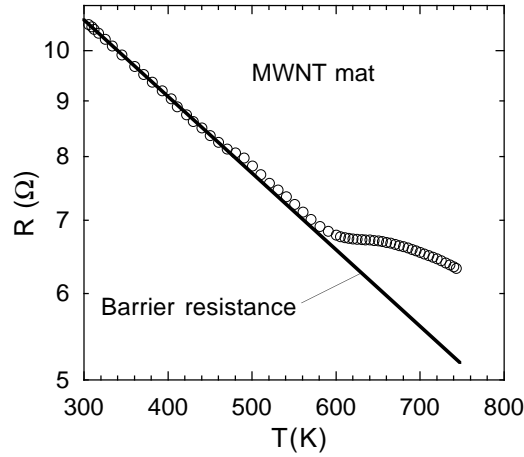


Figure 8. The temperature dependence of the resistance for a MWNT mat. The data are the same as those in Ref. [8] but less data points are plotted for charity. The resistance between 300 K and 450 K can be excellently described by  $17.3\exp(-T/618.3)$  Ω, which represents the intertube barrier resistance [33]. The average diameter of the tubes is about 10 nm.

Figure 8 shows the temperature dependence of the resistance for a MWNT mat. It is interesting that the resistance decreases monotonically with increasing temperature below about 570 K. Above 570 K, the resistance tends to turn up. The resistance between 300 K and 450 K can be excellently described by  $17.3\exp(-T/618.3)$  Ω. This temperature dependence is expected for an intertube barrier resistance [33]. This implies that the on-tube resistance between 300 K and 450 K is negligible, in agreement with several independent

experiments which consistently show a negligible on-tube resistance at room temperature in many individual MWNTs [35, 36, 37, 38]. The observed finite and very small on-tube resistances in the individual MWNTs [37] are consistent with quasi-1D room-temperature superconductivity with finite quantum phase slips.

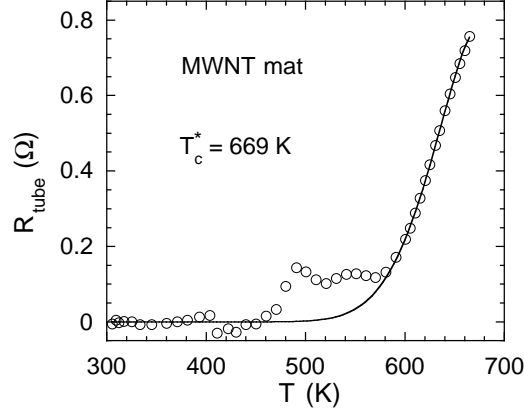


Figure 9. The on-tube resistance by subtracting the barrier resistance from the total resistance of the MWNT mat. The solid line is the fitted curve by Eq. 10 by excluding the data points between 450 K and 600 K. The fitting parameters are  $\beta = 11.34$  and  $T_c^* = 669$  K.

If we assume that this temperature dependence for the intertube barrier resistance remains valid up to 750 K, we then obtain the on-tube resistance by subtracting the barrier resistance from the total resistance. The resultant on-tube resistance below 665 K is shown in Fig. 9. The solid line is the fitted curve by Eq. 10 by excluding the data points between 450 K and 600 K. The shoulder feature between 450 K and 600 K may be caused by quantum phase slips. The fitting parameters are  $\beta = 11.34$  and  $T_c^* = 669$  K. Using the empirical relation  $T_c^* = 0.89T_{c0}$ , we obtain  $T_{c0} = 752$  K.

It is interesting that the value of  $\beta = 11.34$  for this MWNT mat is slightly smaller than that (11.71) for the 12-nm MWNT. This implies that, on average, the total number of transverse channels for each superconducting bundle (which may contain one or more individual MWNTs near  $T_{c0}$ ) is comparable with that for the single 12-nm MWNT. As discussed in section 7., the Josephson coupling among individual MWNTs has not been established near  $T_{c0}$ , so most of the superconducting bundles actually consist of only single MWNT. Only for those small-diameter MWNTs, the Josephson coupling among them is established near  $T_{c0}$  such that several individual tubes are formed into a superconducting bundle. Therefore, the average number of conduction channels per shell should be about 3 for the mat sample, similar to that for the single 12-nm MWNT.

In Fig. 10, we plot the normalized on-tube resistance versus  $T/T_{c0}$  for the 12-nm MWNT ( $T_{c0} = 262$  K) and for the MWNT mat ( $T_{c0} = 752$  K). It is remarkable that the on-tube resistive transitions for the two systems are nearly identical although they have different  $T_{c0}$ 's and the electrical measurements were done by independent groups. This agreement also suggests that both sets of data are reliable and that the procedure to extract the on-tube resistance for the MWNT mat is justified.

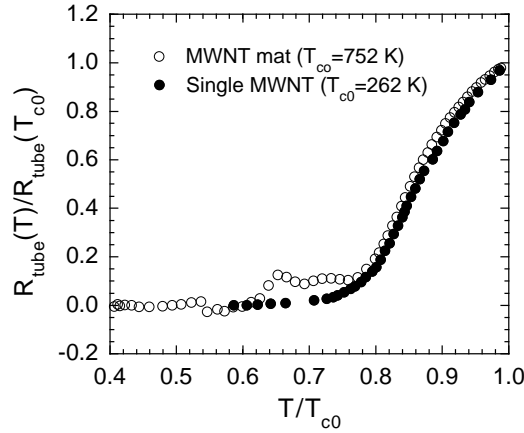


Figure 10. The normalized on-tube resistance versus  $T/T_{c0}$  for the 12-nm MWNT ( $T_{c0} = 262$  K) and for the MWNT mat ( $T_{c0} = 752$  K). The on-tube resistive transitions for the two systems are nearly identical although they have different  $T_{c0}$ 's.

### 3. Magnetic Properties of MWNTs

From the quantitative analyses of the electrical transport data in several carbon nanotubes, we can clearly see that the superconducting transition temperatures can vary from 0.4 K to 750 K for different samples. We believe that the  $T_{c0}$  variation may be associated with the differences in the doping level, the chirality and diameter of tubes, the screening of the long-range Coulomb interaction, and in disorders (see section 7. below). In order to unambiguously show that high-temperature superconductivity in carbon nanotubes is real, one needs to provide magnetic evidence such as the existence of the Meissner effect. However, the Meissner effect may be less visible because the diameters of the tubes may be much smaller than the magnetic penetration depth. Further, the orbital diamagnetic susceptibility in the magnetic field perpendicular to the graphite sheet is large, making it difficult to separate the Meissner effect from the large orbital diamagnetic susceptibility. Fortunately, the orbital diamagnetic susceptibility of carbon nanotubes in the magnetic field parallel to the tube axis is predicted to be very small at room temperature [40]. This makes it possible to extract the Meissner effect from the measured susceptibility in the parallel field.

Figure 11 shows the temperature dependence of the susceptibility for physically separated and aligned MWNTs in a magnetic field parallel to the tube axis. The diameters of the tubes are  $10 \pm 5$  nm, and the lengths are on the order of  $1 \mu\text{m}$ . It is apparent that the diamagnetic susceptibility is significant up to 265 K. Because the orbital diamagnetic susceptibility in the parallel field is negligible at room temperature [40], the observed diamagnetic susceptibility at 265 K should mainly contribute from the Meissner effect due to superconductivity. Thus, the Meissner effect at 265 K is about  $-0.8 \times 10^{-5}$  emu/g, which is significant. This result clearly indicates that the superconducting transition temperature should be higher than 300 K.

For superconducting tubes of radius  $r$  in the magnetic field parallel to the tube axis, the

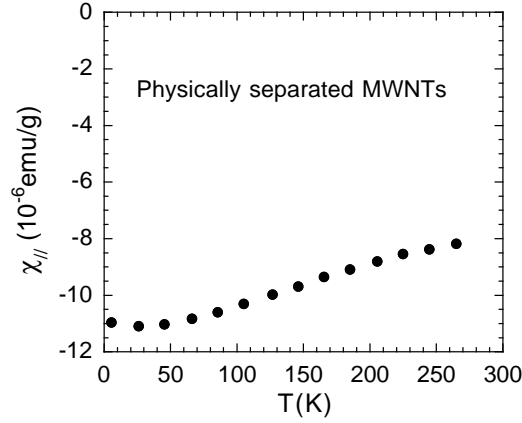


Figure 11. The temperature dependence of the susceptibility for physically separated and aligned MWNTs in a magnetic field parallel to the tube axis. The data are extracted from Ref. [39].

diamagnetic susceptibility due to the Meissner effect is given by

$$\chi_{\parallel}^S(T) = -\frac{\bar{r}^2}{32\pi\lambda_{\theta}^2(T)}. \quad (17)$$

Here  $\bar{r}^2$  is the average value of  $r^2$ , and  $\lambda_{\theta}(T)$  is the penetration depth when carriers move along the circumferential direction. The above equation is valid only if  $\lambda_{\theta}(0)$  is larger than the maximum radius of tubes, which should be the case for carbon nanotubes. Eq. 17 indicates that the Meissner effect is inversely proportional to  $1/\lambda_{\theta}^2(T)$ . Assuming an isotropic gap and taking  $T_{c0} = 752$  K, we find that  $1/\lambda_{\theta}^2(T)$  and thus  $\chi_{\parallel}^S(T)$  are nearly independent of temperature below 265 K. Then we have  $\chi_{\parallel}^S(0) = \chi_{\parallel}(265 \text{ K}) \simeq -0.8 \times 10^{-5}$  emu/g. If we assume that the radii of tubes are equally distributed from 0 to 100 Å, we find  $\bar{r} = 50$  Å and  $\bar{r}^2 = 3333$  Å<sup>2</sup>. With the weight density of 2.17 g/cm<sup>3</sup> (Ref. [41]) and  $\chi_{\parallel}^S(0) = -0.8 \times 10^{-5}$  emu/g, we calculate  $\lambda_{\theta}(0) \simeq 1380$  Å. This value of the penetration depth corresponds to  $n/m_{\theta}^* = 1.48 \times 10^{21}/\text{cm}^3 m_e$ , where  $n$  is the carrier density,  $m_{\theta}^*$  is the effective mass of carriers along the circumferential direction. If we take  $m_{\theta}^* = 0.012 m_e$ , typical for graphites [42], we estimate  $n = 1.78 \times 10^{19}/\text{cm}^3$ , in good agreement with the Hall effect measurement [33] which gives  $n = 1.6 \times 10^{19}/\text{cm}^3$ . It is worthy of noting that the Hall coefficient in the physically separated MWNTs does not go to zero below  $T_{c0}$ . This is because the on-tube resistance does not exactly go to zero due to quantum phase slips and because the magnetic field is almost penetrated into the whole volume of the tubes.

From Eq. 17, we can see that  $\chi_{\parallel}^S(T)$  will increase linearly with increasing  $\bar{r}^2$  or cross-sectional area. For Josephson coupled MWNT bundles in unprocessed mats, the effective  $\bar{r}^2$  is larger than that for physically separated tubes. As the temperature decreases, the Josephson coupling strength increases so that the effective  $\bar{r}^2$  and thus  $\chi_{\parallel}^S(T)$  also increase. This can naturally explain why the diamagnetic susceptibility for physically coupled MWNTs is larger than that for physically separated MWNTs and why the enhancement in the diamagnetic susceptibility increases significantly with decreasing temperature (see Fig. 11).

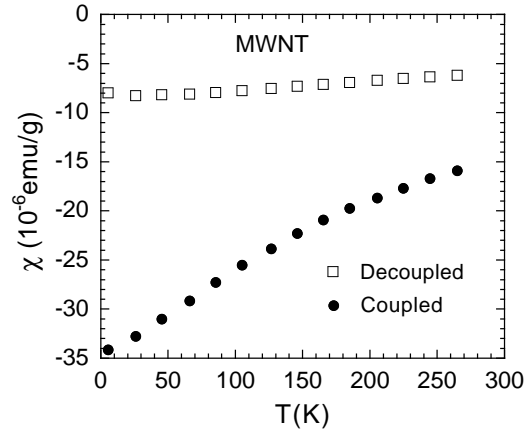


Figure 12. The temperature dependence of the angle-averaged susceptibility for physically separated MWNTs (open squares) and for physically coupled MWNT mat (solid circles). The physically coupled mat sample is not processed so that the tubes are closely packed into bundles. The data are extracted from Ref. [39].

At the lowest temperature, the enhancement factor is about 4.3. Without superconductivity in these MWNTs, it is very difficult to account for such a large enhancement in the diamagnetic susceptibility upon bundling of the tubes.

#### 4. Raman Spectroscopic Evidence for Superconductivity at 665 K

It is known that Raman scattering has provided essential information about the electron-phonon coupling and the electronic pair excitation energy in the high- $T_c$  cuprate superconductors [43, 44, 45]. The anomalous temperature-dependent broadening of the Raman active  $B_{1g}$ -like mode of 90 K superconductors  $\text{R}\text{Ba}_2\text{Cu}_3\text{O}_{7-y}$  (R is a rare-earth element) allows one to precisely determine the superconducting gap [44]. The pronounced softening observed only for the  $B_{1g}$  mode is due to the fact that the phonon energy of the  $B_{1g}$  mode is very close to  $2\Delta(0)$  and the mode is strongly coupled to electrons [44, 46, 47].

The temperature dependence of the frequency for the Raman-active  $B_{1g}$  mode of an optimally doped  $\text{YBa}_2\text{Cu}_3\text{O}_{7-y}$  is shown in Fig. 13a. It is apparent that the frequency decreases linearly with increasing temperature above  $T_c$  and that the mode starts to soften below about  $0.95T_c$ . The temperature dependence of the frequency above  $T_c$  is caused by thermal expansion. The temperature dependence of the frequency will become more pronounced at higher temperatures because the magnitude of the slope  $-d\ln\omega/dT$  is essentially proportional to the lattice heat capacity that increases monotonically with temperature. The significant softening of the mode below  $T_c$  occurs only if the energy of the Raman mode is very close to  $2\Delta(0)$  and the electron-phonon coupling is substantial [46, 47], as it is the case in the optimally doped  $\text{YBa}_2\text{Cu}_3\text{O}_{7-y}$  [43, 44, 45]. In order to see more clearly the softening of the mode, we show in Fig. 13b the difference of the measured frequency and the linearly fitted curve above  $T_c$ . It is clear that the softening starts at about 89 K  $\simeq$

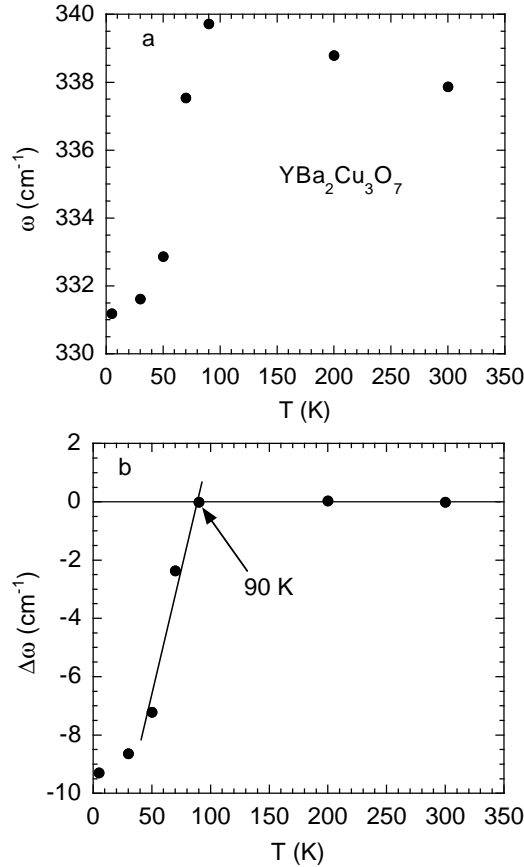


Figure 13. a) The temperature dependence of the frequency for the Raman-active  $B_{1g}$  mode of an optimally doped  $\text{YBa}_2\text{Cu}_3\text{O}_{7-y}$ . The data are extracted from Ref. [43]. b) The difference between the measured frequency and the linearly fitted curve above  $T_c$ .

$0.95T_c$ .

Figure 14a shows the temperature dependence of the frequency for the Raman active graphitic mode of a SWNT mat. It is striking that the frequency data show a clear tendency of softening below about 630 K. Above 630 K, the frequency decreases linearly with increasing temperature with a slope much larger than that in  $\text{YBa}_2\text{Cu}_3\text{O}_{7-y}$ . This is due to a much larger thermal expansion at such high temperatures in SWNTs. The slope will decrease with decreasing temperature and eventually level off at low temperatures. The leveling off between 450-630 K must be due to the competition between the mode hardening due to the normal thermal effect and the mode softening due to a transition to the charge/spin density wave state or to the superconducting state. The transition to the charge/spin density wave state will lead to a metal-insulator transition upon cooling, in contrast to the transport data in Fig. 7 which is only consistent with the superconducting transition.

In order to see more clearly the softening of the mode, we show in Fig. 14b the difference between the measured frequency and the linearly fitted curve above the kink temperature ( $\sim 630$  K). One can see that the result shown in Fig. 14b is similar to that shown in

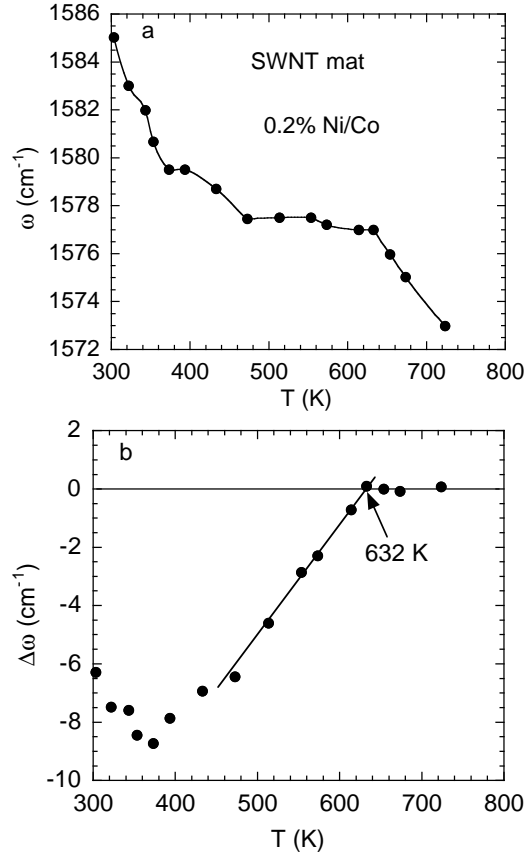


Figure 14. a) The temperature dependence of the frequency for the Raman active graphitic mode of a SWNT mat with 0.2% Ni/Co catalyst. The data are from Ref. [48]. b) The difference of the measured frequency and the linearly fitted curve above the kink temperatures (see text).

Fig. 13b. This suggests that the softening of the Raman active graphitic mode in the SWNTs may have the same microscopic origin as the softening of the Raman active  $B_{1g}$  mode in  $\text{YBa}_2\text{Cu}_3\text{O}_{7-y}$ . This explanation is plausible only if the phonon energy of the graphitic mode is very close to  $2\Delta(0)$ . We are fortunate that the phonon energy of the graphitic mode is 197 meV, very close to  $2\Delta(0) \simeq 200$  meV expected for a  $T_{c0}$  in the range of 600-700 K. If  $T_{c0}$  is away from this range, the phonon self-energy effect will disappear. This can explain why this effect is not visible for another SWNT mat with 1.3% Ni/Co catalyst, as shown in Fig. 15. It is likely that the  $T_{c0}$  of this sample is suppressed to a much lower value by the magnetic impurities.

From Fig. 14, we can clearly see that the softening starts at about 632 K. Using the fact that the softening starts at  $0.95T_{c0}$  (Ref. [46]), we can assign the mean-field transition temperature  $T_{c0} = 665$  K. It is interesting to note that there is a clear minimum at  $T^* = 370$  K  $= 0.57T_{c0}$  in Fig. 14b. Such a minimum is also seen at about  $0.6T_{c0}$  in a calculated curve for a superconductor (see Fig. 8 of Ref. [46]). This shallow minimum in the frequency shift is related to a sharp minimum in the real part of the polarization  $\Pi(\omega, T)$ , which occurs at

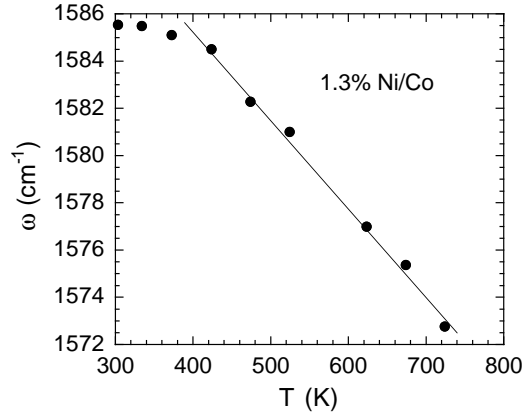


Figure 15. The temperature dependence of the frequency for the Raman active graphitic mode of a SWNT mat with 1.3% Ni/Co catalyst. The data are from Ref. [48]. The phonon self-energy effect is not visible in this sample because the  $T_{c0}$  of the sample might be far away from the range of 600-700 K, which is optimal for the observation of the phonon self-energy effect.

$\hbar\omega/2\Delta(T^*) = 1$  for weak coupling [46, 47]. From the temperature dependence of the BCS gap [17], we find that  $\Delta(T^*) = \Delta(0.57T_{c0}) = 0.93\Delta(0)$ . With  $\hbar\omega/2\Delta(T^*) = 1$  and  $\hbar\omega = 197$  meV, we finally obtain  $\Delta(0) = 106$  meV. Then we calculate  $2\Delta(0)/k_B T_{c0} = 3.7$ , which is in excellent agreement with the prediction based on the plasmon-mediated pairing mechanism [4]. It is worth noting that  $\Delta(0)$  would be much larger if the magnetic impurities would not suppress superconductivity.

We can evaluate the electron-phonon coupling constant for the Raman-active graphitic phonon mode  $\lambda^g$  using a relation [44]:  $\Delta\omega/\omega = 0.5\lambda^g \text{Re}\Pi/N(0)$ . In the weak-coupling limit, the value of  $\text{Re}\Pi/N(0)$  at zero temperature is calculated to be  $-7.0$  using Eq. 16 of Ref. [47] and  $\hbar\omega/2\Delta(0) = 0.93$ . Strong coupling and impurity scattering tend to reduce the magnitude of  $\text{Re}\Pi/N(0)$  [46, 47]. Because  $\Delta\omega/\omega$  is nearly independent of temperature below  $0.45T_{c0}$  [46], we take the value of  $\Delta\omega/\omega$  at zero temperature to be the same as that ( $-0.378\%$ ) at room temperature. Then we obtain  $\lambda^g = 0.0011$  using the relation:  $\Delta\omega/\omega = 0.5\lambda^g \text{Re}\Pi/N(0)$ . The value of  $\lambda^g = 0.0011$  may be slightly underestimated since the coupling to bosonic modes is not in the weak limit ( $2\Delta(0)/k_B T_{c0} = 3.7$ ).

Recently, Lazzeriet al. [49] have used accurate density functional theory (DFT) to compute with high accuracy the electron-phonon coupling for optical phonons in (6, 6) and (11, 11) armchair SWNTs. From their results, we can readily evaluate the electron-phonon coupling constant  $\lambda^g$  for the Raman-active graphitic mode in metallic-chirality SWNTs with different diameters. For  $d = 1.4$  nm, we find that  $\lambda^g = 0.0014$ , in quantitative agreement with that (0.0011) deduced from the superconductivity induced phonon self-energy effect. Such quantitative agreement justifies the above data analyses that suggest a superconducting transition at about 665 K in the SWNT mat sample.

## 5. Tunneling Spectra

One of the important signatures for superconductivity is the existence of the single-particle excitation gap. From a single-particle tunneling spectrum obtained through two high-resistance contacts (see Fig. 1b of Ref. [50]), we can clearly see a pseudo-gap feature which appears at an energy of about 220 meV. The pseudo-gap feature could be related to the superconducting gap. Considering the broadening of the gap feature due to large quantum phase slips and the double tunneling junctions in series, we estimate the superconducting gap  $\Delta(0)$  to be about 100 meV. The scanning tunneling microscopy [51] on individual

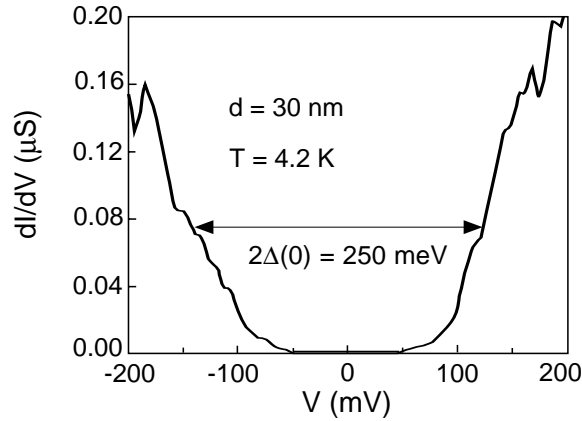


Figure 16. The tunneling spectrum for an “insulating” MWNT with  $d = 30$  nm. The figure is reproduced from Ref. [52]. The energy scale has been reduced by a factor of two compared with the original spectrum for double junctions [52].

single-walled nanotubes also show pseudo-gap features with  $\Delta(0) > 100$  meV in doped metallic SWNTs (the Fermi level  $E_F$  is about 0.2 eV below the charge neutrality point). From the Raman data for a SWNT mat, we have quantitatively deduced  $\Delta(0) = 106$  meV from the phonon self-energy effect. These data consistently suggest that the magnitude of  $\Delta(0)$  can be larger than 100 meV in SWNTs.

For MWNTs, the electrical transport data indicate superconductivity at about 750 K. This implies that the magnitude of  $\Delta(0)$  should be about 120 meV according to  $2\Delta(0)/k_B T_{c0} = 3.7$ . The expected single-particle excitation gap has been seen in the tunneling spectrum for an “insulating” MWNT with  $d = 30$  nm, which is shown in Fig. 16. In the figure, the energy scale has been reduced by a factor of two compared with the original spectrum for double junctions. This spectrum would imply a semiconducting gap of about 200 meV if the outermost shell had a semiconducting chirality. However, according to a formula  $E_g = 2a_{C-C}\gamma_0/d$  (Ref. [20]), the predicted semiconducting gap  $E_g$  for a semiconducting chirality tube with  $d = 30$  nm should be about 22 meV, which is about one order of magnitude smaller than the observed value for the “insulating” tube. In fact, the tunneling spectrum for another “conducting” tube with the same diameter [52] is consistent with  $E_g \simeq 20$  meV (see Fig. 17), suggesting that the “conducting” tube has a semiconducting chirality.

In order to consistently explain the tunneling spectra, we must assume that the “insu-

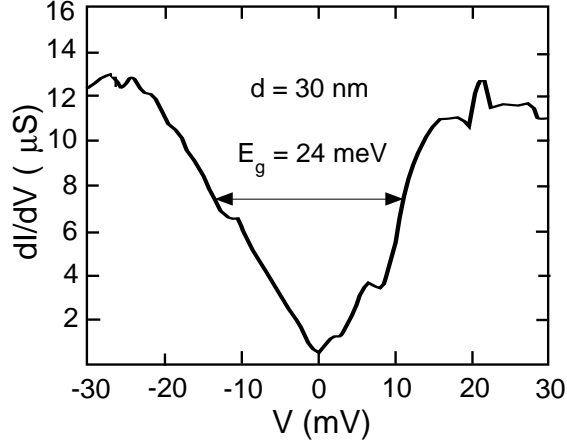


Figure 17. The tunneling spectrum for a “conducting” MWNT with  $d = 30$  nm. The figure is reproduced from Ref. [52]. The magnitude of the gap is consistent with a semiconducting chirality tube.

lating” tube has a metallic chirality and that the gap is related to either the superconducting state or the insulating CDW state. If the gap is related to the insulating ground state, one should be able to observe a rectification effect in a heterojunction between this “insulating” MWNT and another “conducting” MWNT. Indeed, the rectification effect is observed [52] below about 192 K. However, the rectification effect disappears [52] above 192 K, which cannot be explained if the metallic-chirality tube remains insulating. Therefore there must be a transition from the superconducting to the insulating state below  $T_{loc} \simeq 192$  K. A similar transition at about 200 K has been seen in an 18-nm MWNT [27] (see section 2.). Such a transition can occur in dirty quasi-1D systems [30] where the Cooper pairs get localized below  $T_{loc}$ . It is clear that the single-particle gap remains essentially unchanged across  $T_{loc}$ . Therefore, the superconducting gap would be about 125 meV if this 30-nm MWNT were clean enough to avoid the Anderson localization.

The single-particle tunneling spectrum for another MWNT with  $d = 17$  nm is displayed in Fig. 18. It is apparent that both the intensity and the peak position in this spectrum is inconsistent with the normal-state density of states for any types of metallic-chirality tubes [53, 54]. On the other hand, this spectrum is very similar to the one for a superconductor with a superconducting gap of about 54.4 meV.

We can quantitatively explain this spectrum by invoking superconductivity. The peak positions denoted by 1, 2, 3, 4, 5 are located at  $< -117$  mV,  $-54.4$  mV,  $54.4$  mV,  $76.5$  mV, and  $\sim 120$  mV, respectively. Below  $T_{c0}$ , the Van Hove singularities are located at  $\epsilon_{VH} =$

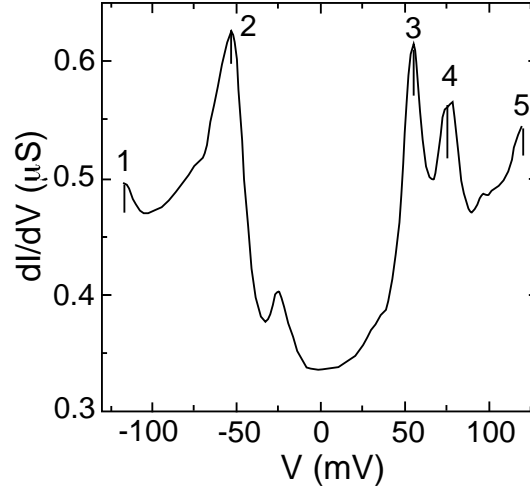


Figure 18. Single-particle tunneling spectrum for a single MWNT with  $d \simeq 17$  nm, which is reproduced from Ref. [21].

$\pm \sqrt{[\Delta(0)]^2 + (E_{VH} - E_F)^2}$ . Here the sign in the prefactor of the square root is the same as the sign of  $E_{VH} - E_F$ . In order to get a consistent explanation to the spectrum, we assume that the tube is hole doped (i.e.,  $E_F < 0$ ) and that the positive voltage corresponds to the negative electron energy.

It is interesting that peak 2 is broader than peak 3. This indicates that peak 2 corresponds to two overlapped peaks: one is a superconducting quasi-particle peak and another is a Van Hove singularity located slightly above the Fermi level. Peak 3 corresponds to another superconducting quasiparticle peak. From the positions of peak 2, 3, and 4, we deduce that  $\Delta(0) = 54.4$  meV,  $E_{VH1} = \pm 54.4$  meV,  $E_{VH2} = \pm 108.5$  meV  $\simeq 2E_{VH1}$ , and  $E_F = -55.0$  meV. The positions of Van Hove singularities agree with the theoretical prediction for an armchair tube [20]. With the values of  $E_{VH1}$ ,  $E_{VH2}$  and  $\Delta(0)$ , we can predict the other peak positions. For example, we predict  $V_1 = -121.6$  mV and  $V_5 = +121.6$  mV, in excellent agreement with the measured results. Using  $E_{VH1} = 54.4$  meV,  $d = 17$  nm, and the relation  $E_{VH1} = 3a_{C-C}\gamma_0/d$  (Ref. [20]), we find that  $\gamma_0 = 2.2$  eV, in quantitative agreement with another independent measurement [55]. It is remarkable that the value of  $\gamma_0 = 2.2$  eV also agrees quantitatively with those deduced from the resistive transitions for both SWNT bundle and individual MWNT (see section 2.).

Since the Fermi level is right on the first Van Hove singularity in this MWNT, the large enhancement in the density of states due to the Van Hove singularity leads to a large increase in the condensation energy, and thus a large suppression of quantum phase slips [10]. The observed sharp quasiparticle peak at the gap edge should be related to substantially reduced quantum phase slips. The much lower gap in the outermost layer of this MWNT is due to the fact that electron-plasmon coupling is significantly reduced when the second subband is crossed [4].

## 6. Negligible on-Tube Resistances in MWNTs

In order to confirm superconductivity at room temperature in a 3D bulk sample, one needs to show zero on-tube resistance at room temperature. However, the on-tube resistance for a quasi-1D superconducting tube with a finite number of transverse channels will never go to zero at finite temperatures due to quantum phase slips [16]. The resistance at room temperature should be negligibly small if  $N_{ch}$  is not too small. Indeed, negligible on-tube resistances have been observed in a multi-walled nanotube bundle consisting of two MWNTs with a diameter  $d = 16$  nm (Ref. [35]), in an individual MWNT with  $d = 40$  nm (Ref. [36]), in over 50 individual MWNTs [37], as well as in a single-walled nanotube bundle consisting of two SWNTs with  $d = 1.4$  nm (Ref. [56]). These electrical transport data are either consistent with ballistic transport or superconductivity at room temperature.

In order to distinguish between ballistic transport and superconductivity at room temperature, it is essential to reliably estimate the lower limit of the room-temperature resistivity due to inelastic scattering. If we consider inelastic scattering only by the twist mode, the calculated on-tube resistance per unit length per shell is the lower limit. If this lower limit is far larger than the measured values, the ballistic transport mechanism is ruled out.

The on-tube resistance per unit length due to the scattering by the twist mode has been deduced for armchair tubes (n, n) [57]. For a Luttinger parameter  $K_c \leq 1$ , the on-tube resistance per unit length is given by [57]

$$R_{tube}/L = \frac{R_Q}{2} \frac{\gamma(K_c)\Lambda^2}{a\hbar v_F C_t} (\pi a k_B T / \hbar v_F)^{(1+K_c)/2}, \quad (18)$$

where  $\Lambda = n \times 2.92$  eVÅ,  $C_t = n^3 \times 18$  eVÅ,  $a = 2.46$  Å, and

$$\gamma(K_c) = 4\pi^{-2} (K_c)^{1+K_c/2} \sin[\pi(1+K_c)/4] \int_0^\infty dz z / [\sinh(z)]^{(3+K_c)/2}. \quad (19)$$

One can easily show that  $\gamma(1) = 2/\pi$  and  $\gamma(0.2) = 0.125$ . Using the relation  $d = (\sqrt{3}/\pi)an$  and  $\hbar v_F = 5.3$  eVÅ, and from Eq. 18, we calculate  $R_{tube}/L$  at room temperature as a function of  $d$  for  $K_c = 1$  and 0.2. The result is shown in Fig. 19. We can see that for  $d = 20$  nm, the on-tube resistance per unit length at room temperature would be at least 275  $\Omega/\mu\text{m}$  if the tube were not superconducting. Other inelastic scattering will further increase the resistivity. For example, the phonon energy of the breathing mode for the 20-nm tube is only 1.4 meV and this mode is strongly coupled to electrons [58]. Such a soft mode will produce a large inelastic scattering at room temperature.

Poncharal *et al.* [37] have made extensive transport studies on over 50 individual MWNTs with diameters ranging from 5 to 25 nm. These MWNTs, which protrude from unprocessed arc produced nanotube fibers and are contacted with liquid metals, show very small per unit length resistances at room temperature:  $R_{tube}/L = 31 \pm 61$   $\Omega/\mu\text{m}$ . For example,  $R_{tube}/L = 14$   $\Omega/\mu\text{m}$  for a MWNT with  $d \simeq 20$  nm. Since the tunneling resistance is close to  $R_Q$  and the electrical contacts are nearly ideal, the current would only flow the outermost shell if the MWNT were not a superconductor. This implies that the value of  $R_{tube}/L$  for the outermost shell ( $d \simeq 20$  nm) would be about 14  $\Omega/\mu\text{m}$ , which is over one order of magnitude smaller than the lower limit (275  $\Omega/\mu\text{m}$ ) expected from the ballistic

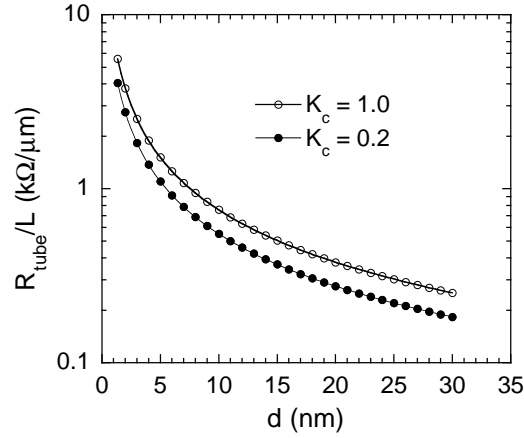


Figure 19. The calculated lower limit of the room-temperature on-tube resistance per unit length  $R_{tube}/L$  as a function of the tube diameter  $d$  for the Luttinger parameter  $K_c = 1.0$  and  $0.2$ . The lower limit is set by the resistivity contributed only from the scattering of a twist mode.

transport mechanism. Therefore, the ballistic transport mechanism cannot explain such a small on-tube resistance at room temperature.

Using the average  $R_{tube}/L = 31 \Omega/\mu\text{m}$  and the average  $d = 15 \text{ nm}$ , and assuming that the current flows through all the shells, we estimate the room-temperature resistivity to be  $5.5 \times 10^{-7} \Omega\text{cm}$ . The resistivity is about 3 orders of magnitude smaller than the normal-state resistivity in the SWNT mat and the single MWNT (see section 2.). The very small but non-zero resistivity is consistent with the existence of quantum phase slips due to a finite number of transverse channels. The quantum-phase slip theory [16, 10] can also account for semiconductor-like temperature dependence of the resistance below room temperature in some MWNTs that are lithographically contacted [21]. The lithographically contacted MWNTs may contain high density of defects or imperfections which are introduced through purification and other processing steps [37]. Defects and disorders enhance quantum-phase slips and localization of Cooper pairs, which would lead to a large on-tube resistance and a semiconductor-like temperature dependence of the resistance well below  $T_{c0}$  (Ref. [16, 10]).

The other important issue to be addressed is why the the tunneling resistance is close to  $R_Q$  rather than  $R_Q/2$  for the ideal electrical contacts to the outermost shell [35]. A possible explanation is that the metal electrode drives the contact region of the outermost shell to the normal state through the proximity effect, which can destroy the Josephson coupling between the outermost shell and the inner shells in the contact region. Because the strong coupling between the liquid metal and the outermost shell, the band with  $\pi$  character is pushed down below the Fermi level, and thus only one channel with  $\pi^*$  character contributes to electrical transport [59].

## 7. Microscopic Pairing Mechanism

It has been shown that the low energy physics of an individual metallic single-walled carbon nanotube is equivalent to a ladder system [60] and can be described by Luttinger liquid with an effective interaction parameter  $K_c$ . For unscreened Coulomb interactions,  $K_c$  is calculated to be about 0.2 in the absence of electron-phonon interactions [61]. On the other hand, if electron-phonon interactions are strong and the Coulomb interactions are effectively screened off,  $K_c$  will become larger than 1. Recent theoretical calculation [58] indicates that the strong electron-phonon interaction with the long-wave breathing mode produces a large attractive interaction, which leads to the following formula

$$K_c = \frac{K_c^\circ}{\sqrt{1 - (K_c^\circ)^2 r_B / r}}, \quad (20)$$

where  $K_c^\circ$  is the unrenormalized parameter in the absence of the electron-phonon interaction with the breathing mode and  $r_B = 2.4 \pm 0.9$  Å. If the Coulomb interaction is completely screened off by external gate electrodes, we have  $K_c^\circ \simeq 1$ . If we take  $r = 7$  Å,  $K_c^\circ = 1$ , and  $r_B = 2.4$  Å, we find  $K_c = 1.23$ .

The value of  $K_c$  can be determined from the measured temperature dependence of the on-tube resistance  $R_{tube}(T)$  on the basis of the theoretical prediction of  $R_{tube}(T)$  for a ladder system [30]. The theory [30] predicts that  $R_{tube}(T) \propto T^{2K_c-2}$ . So the two-probe resistance is given by

$$R(T) = R_0 + CT^{2K_c-2}. \quad (21)$$

In Fig. 20, we show the temperature dependences of the resistance at zero gate voltage for two metallic-chirality SWNTs with  $d = 1.5$  nm and 1.7 nm, respectively. The contacts to the nanotubes are nearly ideal with the transmission probability close to 1 (Ref. [62, 63]). In this case, the two-probe resistance approaches 6.45 kΩ if the on-tube resistance approaches zero. It is remarkable that the temperature dependence of the resistance can be well fit by Eq. 21 with  $K_c = 1.86 \pm 0.12$  for  $d = 1.5$  nm and  $K_c = 1.74 \pm 0.06$  for  $d = 1.7$  nm. The large  $K_c$  values for these individual SWNTs suggest that the long-range Coulomb interaction is effectively screened off by the external gate electrodes. Moreover, since  $K_c > 1.5$ , the on-tube resistance is predicted to be zero at zero temperature [30], in good agreement with experiment [62, 63]. Using Eq. 20 and the measured  $K_c$  values, we can deduce  $r_B = 5.5 \pm 0.2$  Å if we take  $K_c^\circ = 1$ , which is significantly larger than that (2.4 Å) estimated theoretically [58].

In order to resolve this discrepancy, we should also consider the electron-phonon interactions with other phonon modes (e.g., short-wave acoustic and optic modes) and the coupling with electronic excitations such as acoustic plasmons [4, 64]. These additional interactions will renormalize  $K_c^\circ$  such that the quantity  $K_c^\circ$  in Eq. 20 may be replaced by the renormalized  $\bar{K}_c^\circ$ , that is,

$$K_c = \frac{\bar{K}_c^\circ}{\sqrt{1 - (\bar{K}_c^\circ)^2 r_B / r}}. \quad (22)$$

If we substitute  $r_B = 2.4$  Å, and the measured  $K_c$  values into Eq. 22, we obtain  $\bar{K}_c^\circ = 1.28$  in both cases. Using this parameter, we can estimate  $K_c$  to be 1.40 and 1.33 for a single-walled tube with  $r = 25$  Å and 50 Å, respectively.

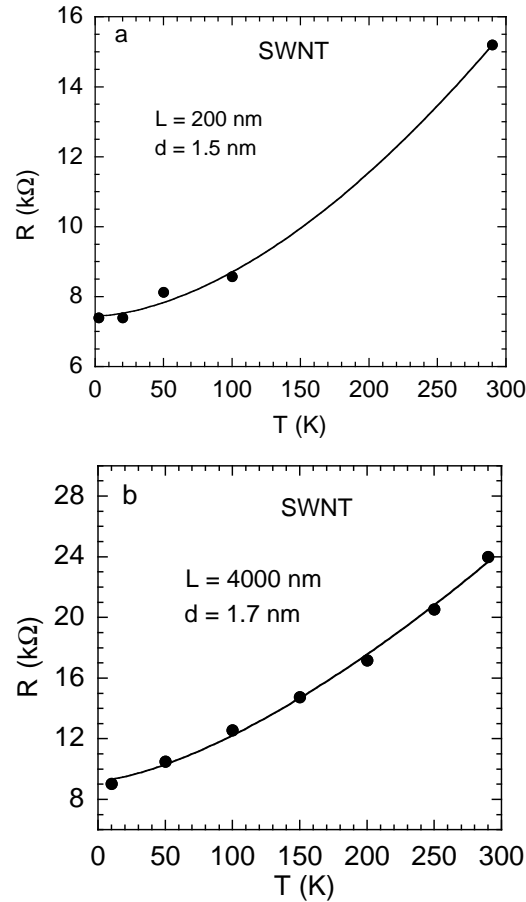


Figure 20. The temperature dependences of the resistance at zero gate voltage for two SWNTs with  $L = 200$  and  $4000$  nm. The data are extracted from Refs. [62, 63].

When individual single-walled nanotubes are closely packed into crystalline bundles, or formed into a multi-walled nanotube, the long-range Coulomb interaction could be reduced by two orders of magnitude [65] depending on the number of tubes comprising the bundles [66]. This implies that the long-range Coulomb interaction in the bulk mat samples can be effectively screened off. Because the short-range on-site  $U$  is reduced by a factor of 10 for an armchair tube with  $d = 1.4$  nm, and the reduction factor is proportional to  $d$  (Ref. [60]), the effective on-site  $U$  becomes very small for a tube with  $d > 1$  nm. Therefore,  $K_c^\circ$  in SWNT mat samples should be close to 1. Moreover, since the intertube coupling will increase  $K_c$  further [58], we expect that  $K_c$  should be about 2 in SWNT mats. For MWNTs, intershell coupling will significantly increase the pairing interaction [5], so the average  $K_c$  in a MWNT with an average shell radius of  $25 \text{ \AA}$  should be much larger than 1.4. For the outermost shell with  $r > 50 \text{ \AA}$ , we may expect  $1.3 < K_c < 1.5$ . If  $K_c < 1.5$  and disorder is significant, the outermost shell will become insulating at low temperatures [30].

Although the strong electron-phonon coupling produces a large attractive interaction, this coupling alone cannot lead to superconductivity above room temperature because of low density of states and low bosonic energies. We believe that electron-plasmon coupling

along with strong electron-phonon coupling should be responsible for high-temperature superconductivity [4, 64]. A SWNT bundle or an individual MWNT is equivalent to a multimode wire. Because the Fermi velocities of the acoustic plasmons in neighboring tubes/shells are comparable, the attractive interaction mediated by undamped acoustic plasmons in the adjacent tubes/shells should be much stronger than that mediated by acoustic phonons [64]. A similar idea has been proposed to explain high-temperature superconductivity in layered cuprates [5]. Within this scenario, high-temperature superconductivity can occur in a multi-layer electronic system due to an attraction of charge carriers in the same conducting layer via exchange of virtual plasmons in neighboring layers [5]. Multi-walled carbon nanotubes and SWNT crystalline bundles are ideal candidates for realization of plasmon-mediated high-temperature superconductivity.

The most favorable conditions for superconductivity are that all the individual tubes comprising MWNTs or SWNT bundles must have metallic chiralities and the chiralities of the adjacent tubes are different. In this situation, the single-particle hopping between neighboring tubes is strongly suppressed [65]. The suppression of the single-particle hopping stems from the obstruction to having precise momentum conservation in the hopping between the misaligned lattices of the nanotubes. This ensures that the single-particle electronic state in individual tubes remains one-dimensional nature such that acoustic plasmon modes remain undamped. This also suppresses any long-range spin or charge ordering because the spin or charge correlation remains one dimensional. On the other hand, the tunneling of Cooper pairs, which is proportional to the square of transverse hopping integral  $t_T$ , turns out to be significant. Because Cooper pairs are formed at zero total momentum, they do not find an obstacle in the tunneling processes from the misalignment of the nanotube lattices. For this reason, one has to take the  $t_T$  value to be the same as that for the case of the perfect alignment [65], that is,  $t_T \simeq 10$  meV for a crystalline bundle composed of 1.4-nm SWNTs [67]. For a bundle consisting of 10 nm SWNTs,  $t_T$  is reduced by a factor of  $\sqrt{10/1.4} = 2.67$  (Ref. [67]), that is,  $t_T \simeq 3.78$  meV. For MWNTs,  $t_T$  should be similar to that for graphites, i.e.,  $t_T \simeq 100$  meV (Ref. [67]).

Now a question arises: Is the Josephson coupling among the individual tubes in a bundle or a MWNT strong enough to sustain phase-coherent superconductivity above room temperature? In order to answer this question, one needs to consider two characteristic temperatures, one is  $T_J$  below which the phase coherence among the tubes takes place, and another is  $T_{c0}$  below which single-particle density of states starts to suppress due to the superconducting correlation in individual tubes. If  $T_J > T_{c0}$  the superconducting transition occurs below  $T_{c0}$ . Otherwise, if  $T_J < T_{c0}$  the superconducting transition occurs below  $T_J$ . We will show that the  $T_J$  values calculated from realistic parameters are significantly higher than 700 K in both SWNT bundles and MWNTs.

The analytical expression for  $T_J$  has been derived within the random-phase-approximation (RPA) [68]. Since the RPA underestimates [68]  $T_J$  by about 20%, we need to multiply the RPA formula by a factor of 1.2 to get a more accurate estimate of  $T_J$ . The modified  $T_J$  formula is then given by [68]

$$T_J = \frac{1.2\Delta(0)}{2\pi} \left[ \frac{2zJ}{\Delta(0)} \sin \pi\delta \frac{\Gamma^2(\delta/2)\Gamma^2(1-\delta)}{\Gamma^2(1-\delta/2)} \right]^{1/(2-2\delta)}, \quad (23)$$

where  $z$  is the number of nearest neighbor tubes,  $\delta = 1/(2K_c)$ ,  $\Delta(0)$  is the single-particle

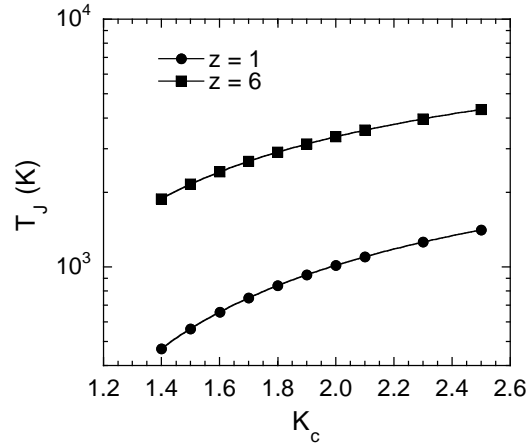


Figure 21. The calculated  $T_J$  as a function of  $K_c$  for SWNT bundles with  $z = 1$  and 6. In the calculation, the following parameters are used:  $\Delta(0)/k_B = 1200$  K,  $t_T = 10$  mV, and  $W = 10$  eV. The value of  $t_T = 10$  meV is suitable for a bundle consisting of SWNTs with  $d = 1.4$  nm [65, 67].  $z = 1$  should correspond to the SWNT mat with  $T_{c0} = 710$  K (see section 2.).

excitation gap (pairing gap), and  $J$  is the intertube Josephson coupling energy which is given by [68]

$$J \simeq \left( \frac{\Delta(0)}{W} \right)^{1/K_c - 1} \frac{t_T^2}{\Delta(0)}, \quad (24)$$

where  $W$  is the order of the original bandwidth. For the SWNT mat with  $T_{c0} = 710$  K, we have shown that, on average, only two superconducting tubes are formed into a bundle, that is, only one of the six nearest neighbor tubes contribute to the Josephson coupling  $J$ . Thus, we can take  $z = 1$  for this special case. From the Raman data, we have found that  $\Delta(0)/k_B = 1200$  K.

Fig. 21 shows the calculated  $T_J$  as a function of  $K_c$  for SWNT bundles with  $z = 1$  and 6. In the calculation we have taken the following parameters:  $\Delta(0)/k_B = 1200$  K,  $t_T = 10$  mV, and  $W = 10$  eV. It is apparent that in order to have  $T_J > T_{c0} = 710$  K for  $z = 1$ , one needs  $K_c > 1.66$ . As we discussed above,  $K_c$  can be larger than 2 for SWNT mats if the long-range Coulomb interaction can be effectively screened off. This implies that the Josephson coupling is strong enough to sustain superconductivity below 710 K. If all the tubes have metallic chiralities and over a hundred tubes are formed into a bundle, quasi-3D superconductivity can be realized well above room temperature. In order to have truly macroscopic superconductivity above room-temperature, one needs over one thousand tubes to comprise a bundle.

For individual MWNTs,  $t_T \simeq 100$  meV if all the shells are superconducting. Even if one third of shells are superconducting,  $t_T$  should be larger than 10 meV. In Fig. 22, we show the calculated  $T_J$  as a function of  $K_c$  with  $t_T = 10$  meV and 100 meV, respectively. In the calculation we have taken the following parameters:  $\Delta(0)/k_B = 1400$  K,  $z = 2$ , and  $W = 10$  eV. For MWNTs,  $z = 2$  and  $\Delta(0)/k_B \simeq 1400$  K (see section 5.). We can see that, in the case of  $t_T = 10$  meV,  $T_J > T_{c0} = 750$  K for  $K_c > 1.43$ . Since the average  $K_c$  in

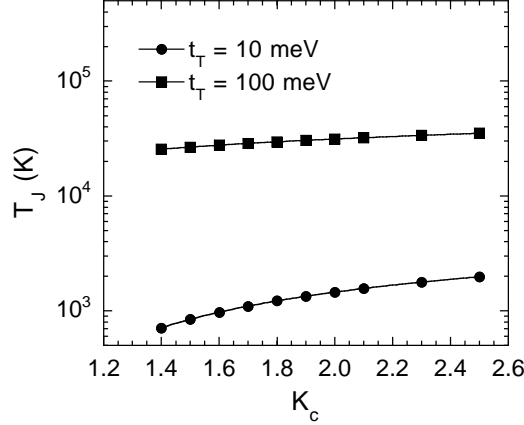


Figure 22. The calculated  $T_J$  as a function of  $K_c$  for individual MWNTs with  $t_T = 10$  meV and 100 meV. In the calculation, the following parameters are used:  $\Delta(0)/k_B = 1400$  K,  $z = 2$ , and  $W = 10$  eV.

MWNTs with  $d = 10$  nm is at least 1.4, the Josephson coupling is strong enough to sustain superconductivity below 750 K. If all the shells have metallic chiralities and over 50 shells are formed into a MWNT, quasi-3D superconductivity can be realized well above room temperature.

For a bundle composed of individual MWNTs with outer diameter of 10 nm, the Josephson coupling temperature  $T_J$  can be calculated with  $t_T = 3.78$  meV (see the above discussion). In Fig. 23, we show the calculated  $T_J$  as a function of  $K_c$  with  $z = 2$  and 6. Because  $K_c$  for the outermost shell should be below 1.5, as discussed above,  $T_J$  is below 500 K even for  $z = 6$ . This implies that the Josephson coupling among the individual MWNTs has not been established near  $T_{c0} = 750$  K. In order to have truly macroscopic superconductivity above room temperature, one needs to bundle the individual MWNTs. But the outer diameters of these tubes should not exceed a critical value, which is about 10 nm according to the result in Fig. 23.

Now let's explain why the  $T_{c0}$ 's in some single-walled nanotube bundles are below 1 K (Ref. [22]). If we check the measured temperature dependence of the normal-state resistance, we find that these bundles behave like semiconductors in the normal state. Assuming that the normal-state resistances of these samples follow Eq. 21, we can estimate the  $K_c$  values from the measured resistances at 1 K and 300 K. We obtain  $K_c \simeq 0.93$  for a SWNT bundle (Pt2) with  $T_{c0} = 0.44$  K, and  $K_c \simeq 0.98$  for another SWNT bundle (Pt1) with  $T_{c0} = 0.15$  K. The values of  $K_c$  indicate that the effective interactions in both bundles are repulsive, leading to d-wave superconductivity [30]. Because the  $K_c$  values are very close to 1, the pairing interaction is weak, leading to low  $T_{c0}$  superconductivity. Since the  $K_c$  value for sample Pt1 is closer to 1 than for sample Pt2, one expects that the repulsive interaction in the former sample is weaker than the latter sample. This can qualitatively explain why the  $T_{c0}$  for sample Pt1 is significantly lower than for sample Pt2. Further, disorder will effectively suppress  $T_{c0}$  for d-wave superconductivity [30]. Because the mean free path of sample Pt2 is one order of magnitude smaller than that of sample Pt1, the  $T_{c0}$  suppression in the former sample is much stronger than in the latter one. Thus, the  $T_{c0}$  difference between samples

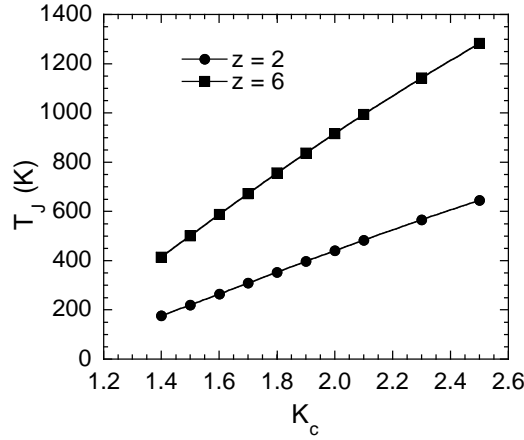


Figure 23. The calculated  $T_J$  as a function of  $K_c$  for a bundle with  $z = 2$  and 6. In the calculation, the following parameters are used:  $\Delta(0)/k_B = 1200$  K,  $t_T = 3.78$  meV, and  $W = 10$  eV. The value of  $t_T = 3.78$  meV is suitable for a bundle composed of tubes with an outer diameter of 10 nm.

Pt1 and Pt2 would even be much greater if the two samples could have similar disorders.

The other important question to be addressed is why these SWNT bundles have  $K_c$  values close to 1. One possibility is that the long-range Coulomb interaction is not effectively screened off for these free-standing samples. The other possibility is that the Fermi levels of these bundle samples are close to the charge neutrality point where the repulsive umklapp interaction cannot be fully ignored and the attractive interaction produced by exchanging short-wave acoustic phonon modes is essentially zero [65, 69]. Indeed, the transport data [62] show that as the Fermi level shifts away from the neutrality point, the  $K_c$  for individual SWNTs can continuously change from  $<1$  to  $>1$ . Therefore, to obtain a large  $K_c$  and high-temperature superconductivity, sufficient doping and effective screening of the long-range Coulomb interaction are essential. Without screening the long-range Coulomb interaction, high-temperature d-wave superconductivity would also occur if the materials were extremely clean. In this case, the electron-phonon and electron-plasmon interactions behave like pair breakers. Moreover, impurities and disorders can easily break pairs and cause Anderson localization of the Cooper pairs [30].

## 8. Pairing Symmetry

The remaining issue to be clarified is the pairing symmetry. In highly oriented pyrolytic graphite (HOPG) samples, there appear to be an interplay between superconductivity and ferromagnetism [70]. Such an interplay suggests that the pairing symmetry in HOPG samples should be of  $p$ -wave, similar to the case of  $\text{Sr}_2\text{RuO}_4$ . Considering the similarity between carbon nanotubes and HOPG, we may expect that the gap symmetry in carbon nanotubes should also be  $p$ -wave. An essential attribute for  $p$ -wave superconductivity is that the spin susceptibility is the same in the superconducting and normal states. The spin susceptibility for aligned and physically separated MWNTs has been derived from electron-

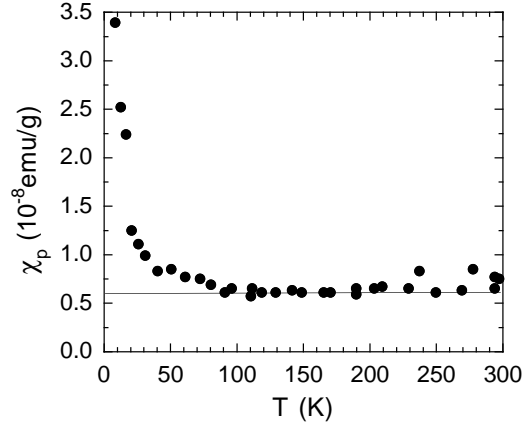


Figure 24. Electron spin susceptibility for a physically separated MWNT film, derived from electron-spin-resonance (ESR) signals. The data are extracted from Ref. [39].

spin-resonance (ESR) signals. Fig. 24 shows the temperature dependence of the spin susceptibility for the MWNTs. The data are extracted from Ref. [39]. It is interesting that the spin susceptibility is independent of temperature between 100 K and 200 K. Below 100 K, the spin susceptibility suddenly turns up and follows a Curie law ( $\propto 1/T$ ) below 40 K. Above 200 K, there appears to be a tendency of increase in the spin susceptibility. From the magnitude of the spin susceptibility between 100 K and 200 K ( $6.0 \times 10^{-9}$  emu/g), one finds that the density of states at the Fermi level  $N(0) = 2.2 \times 10^{-3}$  states/eV atom. The observed finite density of states below 300 K may argue against the interpretation of superconductivity above room temperature in the case of *s*-wave gap symmetry. Nevertheless, the finite density of states is also consistent with *s*-wave gap symmetry if some of the tubes (e.g., semiconducting chirality tubes or shells) are nonsuperconducting.

In order for the *s*-wave interpretation to be plausible, the density of states in the normal state must be significantly larger than that in the superconducting state. Since the spin susceptibility for the film sample was measured only up to room temperature, the normal-state density of states was undetermined. However, if the doping level of the film sample is similar to that for the MWNT mat sample with  $T_{c0} = 752$  K, the normal-state density of states in the film sample should be similar to that for the mat sample. Using the deduced  $\beta$  value from the resistive transition, we have found that the average number of transverse conduction channels per shell is about 3 for the superconducting MWNTs with an average outer diameter of 10 nm (see section 2.). Then  $N(0)$  in the normal state is  $1.5(2\sqrt{3}/\pi^2)(1/\gamma_0)(a_{C-C}/\bar{d})$  (Ref. [20]), where  $a_{C-C} = 0.142$  nm and  $\gamma_0 = 2.4$  eV. The average diameter for all the shells  $\bar{d}$  should be a half of the average outer diameter, that is,  $\bar{d} = 5$  nm. Substituting these numbers into the above formula yields  $N(0) = 6.2 \times 10^{-3}$  states/eV atom. It is clear that the  $N(0)$  in the superconducting state is about one third of that in the normal state, in agreement with *s*-wave gap symmetry.

The finite spin susceptibility in the superconducting state could be partly due to some insufficiently doped semiconducting chirality shells which do not undergo the superconducting transition. Especially for those semiconducting chirality shells in which the Fermi level is in the vicinity of the first Van Hove singularity (near the semiconducting gap edge),

the contribution to the density of states is huge. If one of such shells in a MWNT is present, the density of states contributed from this shell should be comparable with the measured value below 300 K. Moreover, since the Fermi level is also very close to the mobility edge of the semiconducting chirality shell, the charge localization at low temperatures is inevitable. This can naturally explain the upturn of the spin susceptibility below 100 K.

Because the ESR linewidth, which is proportional to the transport scattering rate, also shows upturn below 100 K, there should be one type of carriers responsible for the ESR signals [39]. Since the localized carrier density [39] is only about  $1 \times 10^{18}/\text{cm}^3$  while the mobile carrier density [33] above 100 K is over  $2 \times 10^{19}/\text{cm}^3$ , the majority of the mobile carriers must be ESR-silent, that is, the majority of the mobile carriers are bound into spin singlet pairs.

On the other hand, if there were only one-type of carriers (no superconductivity interpretation), the ESR and Hall effect would measure the same type of carriers. If this were the case, the Hall coefficient would jump to a very large number below 40 K where all the carriers are localized [39]. This is in contrast to the Hall coefficient of the same sample, where no such a jump is seen below 40 K [33]. Moreover, the Fermi energy  $E_F$  would be equal to  $n/N(0) = 4.5$  meV if there were only one-type of carriers. With such a small Fermi energy, one would predict the magnitude of the orbital diamagnetic susceptibility in the perpendicular field [40] to be at least  $1.4 \times 10^{-5}$  emu/g, which is significantly larger than the measured one ( $< 0.7 \times 10^{-5}$  emu/g) [39]. Therefore, there must be two types of carriers; one type of carriers is ESR silent below 300 K due to formation of spin singlet pairs and the other is from nonsuperconducting tubes. A small increase in the spin susceptibility above 200 K may be caused by the thermally excited quasiparticles. If this interpretation is relevant, the minimum superconducting gap is approximately equal to  $200 \text{ K}/0.2 = 1000 \text{ K}$ , in good agreement with the tunneling spectrum (see Fig. 16).

It is worth noting that the observation of the finite spin susceptibility in the superconducting state does not necessarily imply an unconventional pairing symmetry. Even for conventional superconductors such as mercury and tin, the spin susceptibility in the superconducting state is about two thirds of the value in the normal state [71, 72]. For vanadium and aluminum, the spin susceptibility is nearly the same in the superconducting and normal states [72, 73].

## 9. Conclusion

It is well known that copper-based perovskite oxides rightly enjoy consensus as high-temperature superconductors on the basis of two signatures: the resistive transition and the Meissner effect. Here we have provided evidence for room-temperature superconductivity in carbon nanotubes. Although the superconducting transition temperatures can vary from 0.44 K to 750 K, the resistive transitions in these superconducting carbon nanotubes are in quantitative agreement with the Langer-Ambegaokar-McCumber-Halperin theory. The quantitative agreement between the resistive transitions and well established quantum theory leaves little room for alternative explanations. Because of a finite number of transverse conduction channels of these carbon nanotubes, the four-probe resistance will never go to zero in the superconducting state. This would lead to a false impression that these tubes are not superconducting. Nonetheless, the on-tube resistance at room temperature has been

found to be indistinguishable from zero for many individual multi-walled nanotubes. The very small but finite room-temperature on-tube resistance is consistent with quantum phase slips due to the finite number of transverse channels. We have also observed the Meissner effect in aligned and physically separated multi-walled nanotubes up to room temperature. The Meissner effect agrees quantitatively with the predicted magnetic penetration depth from the measured carrier density. Furthermore, the bundling of individual MWNTs into closely packed bundles leads to a large enhancement in the diamagnetic susceptibility, which is the hallmark of the Josephson coupling among the tubes in bundles. Further, Raman data and tunneling spectra consistently show single particle excitation gaps of larger than 100 meV. Therefore, these results consistently indicate quasi-1D room-temperature superconductivity in carbon nanotubes.

For practical applications, zero on-tube resistance at room temperature is required. Although the room-temperature resistivity for individual MWNTs, prepared by arc discharge, is significantly smaller than that for simple elemental metals, we can further suppress the resistivity down to nearly zero by bundling these individual tubes into a big closely packed bundle. But the outer diameters of the tubes should not exceed a critical value above which the magnitude of  $t_T$  is not large enough to sustain the Josephson coupling among the tubes at room temperature. Sufficient doping, effective screening of the long-range Coulomb interaction, and proper bundling are essential to achieve high-temperature superconductivity. Impurities and disorders tend to destroy superconductivity especially in the case of  $K_c < 1.5$ . It is very likely that the  $K_c$  of the outermost shell of a MWNT is less than 1.5 if  $d > 15$  nm. These tubes, if not clean enough, will undergo the superconductor-to-insulator transition below a localization temperature  $T_{loc}$ . For  $K_c > 1.5$ , such a transition should not occur and the ground state is always superconducting.

## References

- [1] Alexandrov, A. S. and Mott, N. F. *Polarons and Bipolarons*, World Scientific, Singapore, 1995.
- [2] Ginzburg, V. L. in: Ginzburg, V. L. and Kirzhnits, D. A. (Eds) *High-Temperature Superconductivity*, Consultants Bureau, New York, 1982.
- [3] Little, W. A. *Phys. Rev.* **164**, A1416 (1964).
- [4] Lee, Y. C. and Mendoza, B. S. *Phys. Rev. B* **39**, 4776 (1989).
- [5] Cui, S. M. and Tsai, C. H. *Phys. Rev. B* **44**, 12500 (1991).
- [6] Saito, R., Fujita, M., Dresselhaus, G., and Dresselhaus, M. S. *Appl. Phys. Lett.* **60**, 2204 (1992).
- [7] Ajiki, H. and Ando, T. *J. Phys. Soc. Jpn.* **62**, 1255 (1992).
- [8] Zhao, G. M. and Wang, Y. S. cond-mat/0111268.
- [9] Zhao, G. M. cond-mat/0208197.

- 
- [10] Zhao, G. M. cond-mat/0208198.
- [11] Zhao, G. M. cond-mat/0208200.
- [12] Zhao, G. M. cond-mat/0208201.
- [13] Zhao, G. M. cond-mat/0307770.
- [14] Zhao, G. M. *Molecular Nanowires and Other Quantum Objects*, Alexandrov, A. S., Demsar J., and Yanson, I. K. (Eds), Nato Science Series, Kluwer Academic Publishers, Netherlands, 2004, page 95-106.
- [15] Langer, J. S. and Ambegaokar, V. *Phys. Rev.* **164**, 498 (1967); McCumber, D. E. and Halperin, B. I. *Phys. Rev. B* **1**, 1054 (1970).
- [16] Zaikin, A. D., Golubev, D. S., Van Otterlo, A., and Zimanyi, G. T. *Phys. Rev. Lett.* **78**, 1552 (1997).
- [17] Tinkham, M. *Introduction to Superconductivity*, McGraw-Hill, 1996.
- [18] Lau, C. N., Markovic, N., Bockrath, M., Bezryadin, A., and Tinkham, M. *Phys. Rev. Lett.* **87**, 217003 (2001).
- [19] Roche, S. and Saito, R. *Phys. Rev. B* **59**, 5242 (1999).
- [20] Mintmire, J. W. and White, C. T. *Phys. Rev. Lett.* **81**, 2506 (1998).
- [21] Schönenberger, C., Bachtold, A., Strunk, C., Salvetat, J.-P., and Forro, L. *Appl. Phys. A* **69**, 283 (1999).
- [22] Kociak, M., Kasumov, A. Yu., Gueron, S., Reulet, B., Khodos, I. I., Gorbatov, Yu. B., Volkov, V. T., Vaccarini, L., and Bouchiat, H. *Phys. Rev. Lett.* **86**, 2416 (2001).
- [23] Trucker, J. R. and Halperin, B. I. *Phys. Rev. B* **3**, 3768 (1971).
- [24] Bendedict, L. X., Crespi, V. H., Louie, S. G., and Cohen, M. L. *Phys. Rev. B* **52**, 14935 (1995).
- [25] Mintmire, J. W., Dunlap, B. I., and White, C. T. *Phys. Rev. Lett.* **68**, 631 (1992).
- [26] Ferrier, M., De Martino, A., Kasumov, A., Gueron, S., Kociak, M., Egger, R., and Bouchiat, H. cond-mat/0405449.
- [27] Ebbesen, T. W., Lezec, H. J., Hiura, H., Bennett, J. W., Ghaemi, H. F., and Thio, T. *Nature (London)* **382**, 54 (1996).
- [28] Private communications with Prof. T. W. Ebbesen.
- [29] Saito, R., Fujita, M., Dresselhaus, G., and Dresselhaus, M. S. *Phys. Rev. B* **46**, 1804 (1992).
- [30] Orignac, E. and Giamarchi, T. *Phys. Rev. B* **56**, 7167 (1997).

- 
- [31] Lee, R. S., Kim, H. J., Fischer, J. E., Thess, A., and Smalley, R. E. *Nature* (London) **388**, 255 (1997).
- [32] Merchant, L., Ostrick, J., Barber, Jr. R. P., and Dynes, R. C. *Phys. Rev. B* **63**, 134508 (2001).
- [33] Baumgartner, G., Carrard, M., Zuppiroli, L., Bacsá, W., De Heer, W. A., and Forro, L. *Phys. Rev. B* **55**, 6704 (1997).
- [34] Stahl, H., Appenzeller, J., Martel, R., Avouris, Ph., and Lengeler, B. *Phys. Rev. Lett.* **85**, 5186 (2000).
- [35] Frank, S., Poncharal, P., Wang, Z. L., De Heer, W. A. *Science* **280**, 1744 (1998).
- [36] De Pablo, P. J., Graugnard, E., Walsh, B., Andres, R. P., Datta, S., and Reifengergera, R. *Appl. Phys. Lett.* **74**, 323 (1999).
- [37] Poncharal, P., Berger, C., Yi, Y., Wang, Z. L., de Heer, W. A. *J. Phys. Chem. B* **106**, 12104 (2002).
- [38] Urbina, A., Echeverra, I., Perez-Garrido, A., Daz-Sanchez, A., and Abellan, J. *Phys. Rev. Lett.* **90**, 106603 (2003).
- [39] Chauvet, O., Forro, L., Bacsá, W., Ugarte, D., Doudin, B., and De Heer, W. A. *Phys. Rev. B* **52**, R6963 (1995). The aligned nanotube films were produced by a process in which the tubes are ultrasonically separated.
- [40] Lu, J. P. *Phys. Rev. Lett.* **74**, 1153 (1995).
- [41] Qian, D., Dickeya, E. C., Andrews, R., and Rantell, T. *Appl. Phys. Lett.* **76**, 2868 (2000).
- [42] Bayot, V., Piraux, L., Michenaud, J.-P., and Issi, J.-P. *Phys. Rev. B* **40**, 3514 (1989).
- [43] Krantz, M., Rosen, H. J., Macfarlane, R. M., and Lee, V. Y. *Phys. Rev. B* **38**, 4992 (1988).
- [44] Friel, B., Thomsen, C., and Cardona, M. *Phys. Rev. Lett.* **65**, 915 (1990).
- [45] Ham, K. M., Kim, J. T., Sooryakumar, R., and Lemberger, T. R. *Phys. Rev. B* **47**, 11 439 (1993).
- [46] Zeyher, R. and Zwicknagl, G. *Z. Phys. B* **78**, 175 (1990).
- [47] Zeyher, R. and Zwicknagl, G. *Solid State Commun.* **66**, 617 (1988).
- [48] Walter, R. *et al.*, *Bull Am. Phys. Soc.* **47**, 361 (2002); The Raman data were sent by Dr. R. Walter from the University of North Carolina.
- [49] Lazzeri, M., Piscanec, S., Mauri, F, Ferrari, A. C., and Robertson, J. *Phys. Rev. Lett.* **95**, 236802 (2005).

- 
- [50] Yao, Z., Kane, C. L., and Dekker, C. *Phys. Rev. Lett.* **84**, 2941 (2000).
- [51] Wildoer, J. W. G., Venema, L. C., Rinzler, A. G., Smalley, R. E., and Dekker, C. *Nature* (London) **391**, 59 (1998).
- [52] Kim, J., Lee, J.-O., Oh, H., Yoo, K.-H., and Kim, J.-J. *Phys. Rev. B* **64**, 161404R (2001).
- [53] Kwon, Y. K. and Tomanek, D. *Phys. Rev. B* **58**, R16001 (1998).
- [54] Sanvito, S., Kwon, Y.-K., Tomanek, D., and Lambert, C. J. *Phys. Rev. Lett.* **84**, 1974 (2000).
- [55] Collins, P. G., Arnold, M. S., and Avouris, P. *Science* **292**, 706 (2001).
- [56] Bachtold, A., Fuhrer, M. S., Plyasunov, S., Forero, M., Anderson, E. H., Zettl, A., and McEuen, P. L. *Phys. Rev. Lett.* **84**, 6082 (2000).
- [57] Komnik, A. and Egger, R. cond-mat/9906150 (1999).
- [58] De Martino, A. and Egger, R. *Phys. Rev. B* **67**, 235418 (2003).
- [59] Choi, H. J. Ihm, J., Yoon, Y.-G., and Louie, S. G. *Phys. Rev. B* **60**, R14009 (1999).
- [60] Balents, L. and Fisher, M. P. A. *Phys. Rev. B* **55**, 11973 (1997).
- [61] Kane, C., Balents, L., and Fisher, M. P. A. *Phys. Rev. Lett.* **79**, 5086 (1997).
- [62] Kong, J., Yenilmez, E., Tomblar, T. W., Kim, W., Dai, H. J., Laughlin, R. B., Liu, L., Jayanthi, C. S., and Wu, S. Y. *Phys. Rev. Lett.* **87**, 106801 (2001).
- [63] Mann, D. Javey, A. Kong, J. Wang, Q., and Dai, H. *Nano Lett.* **3**, 1541 (2003).
- [64] Loss, D. and Martin, T. *Phys. Rev. B* **50**, 12 160 (1994).
- [65] Gonzalez, J., *Phys. Rev. B* **67**, 014528 (2003).
- [66] Alvarez, J. V., and Gonzalez, J. *Phys. Rev. Lett.* **91**, 076401 (2003).
- [67] Maarouf, A. A., Kane, C. L., and Mele, E. J. *Phys. Rev. B* **61**, 11 156 (2000).
- [68] Carr, S. T. and Tselik, A. M. *Phys. Rev. B* **65**, 195121 (2002).
- [69] Sedeki, A., Caron, L. G., and Bourbonnais, C. *Phys. Rev. B* **65**, 140515R (2002).
- [70] Kopelevich, Y., Esquinazi, P., Torres, J. H. S., and Moehlecke, S. J. *Low Temp. Phys.* **119**, 691 (2000).
- [71] Reif, F., *Phys. Rev.* **106**, 208 (1957).
- [72] Androes, G. M. and Knight, W. D. *Phys. Rev. Lett.* **2**, 386 (1959).
- [73] Noer R. J. and Knight, W. D. *Rev. Mod. Phys.* **36**, 177 (1964).